NASA/TM—2012-217743

# An Empirical Temperature Variance Source Model in Heated Jets

*Abbas Khavaran*
*Science Applications International Corporation, Cleveland, Ohio*

*James Bridges*
*Glenn Research Center, Cleveland, Ohio*

October 2012

# NASA STI Program . . . in Profile

Since its founding, NASA has been dedicated to the advancement of aeronautics and space science. The NASA Scientific and Technical Information (STI) program plays a key part in helping NASA maintain this important role.

The NASA STI Program operates under the auspices of the Agency Chief Information Officer. It collects, organizes, provides for archiving, and disseminates NASA's STI. The NASA STI program provides access to the NASA Aeronautics and Space Database and its public interface, the NASA Technical Reports Server, thus providing one of the largest collections of aeronautical and space science STI in the world. Results are published in both non-NASA channels and by NASA in the NASA STI Report Series, which includes the following report types:

- TECHNICAL PUBLICATION. Reports of completed research or a major significant phase of research that present the results of NASA programs and include extensive data or theoretical analysis. Includes compilations of significant scientific and technical data and information deemed to be of continuing reference value. NASA counterpart of peer-reviewed formal professional papers but has less stringent limitations on manuscript length and extent of graphic presentations.

- TECHNICAL MEMORANDUM. Scientific and technical findings that are preliminary or of specialized interest, e.g., quick release reports, working papers, and bibliographies that contain minimal annotation. Does not contain extensive analysis.

- CONTRACTOR REPORT. Scientific and technical findings by NASA-sponsored contractors and grantees.

- CONFERENCE PUBLICATION. Collected papers from scientific and technical conferences, symposia, seminars, or other meetings sponsored or cosponsored by NASA.

- SPECIAL PUBLICATION. Scientific, technical, or historical information from NASA programs, projects, and missions, often concerned with subjects having substantial public interest.

- TECHNICAL TRANSLATION. English-language translations of foreign scientific and technical material pertinent to NASA's mission.

Specialized services also include creating custom thesauri, building customized databases, organizing and publishing research results.

For more information about the NASA STI program, see the following:

- Access the NASA STI program home page at *http://www.sti.nasa.gov*

- E-mail your question to *help@sti.nasa.gov*

- Fax your question to the NASA STI Information Desk at 443–757–5803

- Phone the NASA STI Information Desk at 443–757–5802

- Write to:
  STI Information Desk
  NASA Center for AeroSpace Information
  7115 Standard Drive
  Hanover, MD 21076–1320

NASA/TM—2012-217743

# An Empirical Temperature Variance Source Model in Heated Jets

*Abbas Khavaran*
*Science Applications International Corporation, Cleveland, Ohio*

*James Bridges*
*Glenn Research Center, Cleveland, Ohio*

National Aeronautics and
Space Administration

Glenn Research Center
Cleveland, Ohio 44135

October 2012

## Acknowledgments

This work was sponsored by the NASA Fundamental Aeronautics Program. The authors are grateful to the Acoustics Branch, NASA Glenn Research Center for supporting this research, and to Drs. Stewart Leib and James Debonis for their constructive comments and suggestions. The authors also acknowledge Mr. V.A. Bhagwandin, currently with the U.S. Army Research Laboratory in Aberdeen Maryland, for providing the Wind-US solution to the jet configurations listed in Table 2.

This report is a formal draft or working paper, intended to solicit comments and ideas from a technical peer group.

This report contains preliminary findings, subject to revision as analysis proceeds.

This work was sponsored by the Fundamental Aeronautics Program at the NASA Glenn Research Center.

*Level of Review*: This material has been technically reviewed by technical management.

Available from

NASA Center for Aerospace Information
7115 Standard Drive
Hanover, MD 21076–1320

National Technical Information Service
5301 Shawnee Road
Alexandria, VA 22312

Available electronically at http://www.sti.nasa.gov

# An Empirical Temperature Variance Source Model in Heated Jets

Abbas Khavaran
Science Applications International Corporation
Cleveland, Ohio 44135

James Bridges
National Aeronautics and Space Administration
Glenn Research Center
Cleveland, Ohio 44135

## ABSTRACT

An acoustic analogy approach is implemented that models the sources of jet noise in heated jets. The equivalent sources of turbulent mixing noise are recognized as the differences between the fluctuating and Favre-averaged Reynolds stresses and enthalpy fluxes. While in a conventional acoustic analogy only Reynolds stress components are scrutinized for their noise generation properties, it is now accepted that a comprehensive source model should include the additional *entropy source* term. Following Goldstein's generalized acoustic analogy, the set of Euler equations are divided into two sets of equations that govern a non-radiating base flow plus its residual components. When the base flow is considered as a locally parallel mean flow, the residual equations may be rearranged to form an inhomogeneous third-order wave equation. A general solution is written subsequently using a Green's function method while all non-linear terms are treated as the equivalent sources of aerodynamic sound and are modeled accordingly.

In a previous study, a specialized Reynolds-averaged Navier-Stokes (RANS) solver was implemented to compute the variance of thermal fluctuations that determine the enthalpy flux source strength. The main objective here is to present an empirical model capable of providing a reasonable estimate of the stagnation temperature variance in a jet. Such a model is parameterized as a function of the mean stagnation temperature gradient in the jet, and is evaluated using commonly available RANS solvers. The ensuing thermal source distribution is compared with measurements as well as computational result from a dedicated RANS solver that employs an enthalpy variance and dissipation rate model. Turbulent mixing noise predictions are presented for a wide range of jet temperature ratios from 1.0 to 3.20.

## Nomenclature

| | |
|---|---|
| $c$ | Sound speed |
| $C_\ell, C_\tau$ | Empirical constants |
| $D_j$ | Jet diameter |
| $h$ | Enthalpy |
| $h_t$ | Stagnation enthalpy ( $h + v^2/2$ ) |
| $\vec{k}$ | Wave number |
| $k$ | Wave number magnitude $(\omega/c_\infty)$ |
| $\kappa$ | Turbulent kinetic energy |
| $\varepsilon$ | Turbulent dissipation rate |
| $\ell$ | Turbulence length-scale |
| $M_a$ | Acoutsic Mach number $(U/c_\infty)$ |
| $M_j$ | Aerodynamic Mach number at jet exit |

| | |
|---|---|
| $NPR$ | Nozzle plenum pressure ratio |
| $NTR$ | Nozzle plenum temperature ratio |
| $\omega$ | Radian frequency $(2\pi f)$ |
| $m_j$ | Momentum variable $(\rho v_j')$ |
| $\pi'$ | Normalized pressure fluctuation |
| $\rho$ | Density |
| $p$ | Pressure |
| $P_{ref}$ | Reference acoustic pressure (0.0002 μbar) |
| $R$ | Arc distance from jet exit |
| $r$ | Radial distance from jet centerline |
| $\Re$ | Gas constant |
| $\vec{\xi}$ | Spatial separation vector |
| $t$ | Time |
| $\tau$ | Time delay |
| $\tau_o$ | Turbulence time-scale |
| $U$ | Mean axial velocity |
| $v_i$ | Velocity components |
| $v_i'$ | Turbulent velocity component |
| $\theta$ | Polar angle from downstream axis |
| $\vec{x}$ | Observer location |
| $\vec{y}$ | Source location |
| $\delta_{ij}$ | Kronecker delta |

Subscripts

| | |
|---|---|
| $c$ | Convection variable |
| $\infty$ | Ambient condition |
| $t$ | Stagnation value |
| $j$ | Jet exit conditions |

Superscripts

| | |
|---|---|
| – | Time average |
| ~ | Favre average ( $\tilde{q} = \overline{\rho q} / \bar{\rho}$ ) |
| $\langle\,\rangle$ | Variance |
| ′ | Fluctuating quantity |
| $s$ | Source location |

## 1.0 Introduction

The Fundamental Aeronautics program at NASA is tasked with achieving technological capabilities necessary to overcome air transportation challenges that include reduced noise, emissions, and fuel consumption. The U.S. commercial aviation traffic is projected to increase by 70% in the period 2010 – 2030; subsequently more people will be exposed to air traffic noise in the communities surrounding airports. Recent noise metrics require a cumulative (cutback, sideline and approach) noise reduction in the subsonic transport of 32dB by 2015 and 71dB by 2025 (referenced to 737-800 aircraft with CFM56 engines). Drastic changes in both propulsion system and engine placement are required to achieve these objectives. Computational tools are under research and development that address component noise from a host of structural components such as wing flaps, slats, landing gears, as well as propulsion system elements such as engine inlet, combustion and exhaust noise. Today's high bypass ratio engines

have mitigated jet noise substantially such that jet noise during takeoff is now slightly less than fan exhaust-noise, and is nearly on par with fan noise along the sideline. In this article, we primarily focus on the turbulence-generated noise that is a product of the mixing of the jet exhaust flow with the surrounding air. Since jet mixing-noise is broadband with significant levels of noise within a three-octave frequency band, a successful predictive capability needs to incorporate sufficient physics to produce a reasonably accurate spectrum over a broad range of conditions.

As part of an ongoing research effort at the NASA Glenn Research Center, a RANS-based jet noise prediction methodology (also referred to as physics-based) is being developed to provide the state-of-the-art in source modeling and propagation. The goal is to achieve practical levels of accuracy in noise prediction from a generalized modeling methodology to help designers with concept evaluation and down selection within a reasonable time frame. Physics-based prediction methods have an advantage over the empirical models when design concepts fall outside the envelope of the latter method. Empirical models, on the other hand, are computationally efficient and may be more advantageous when noise is one component in a more general system study.

There have been numerous efforts in the past half-century to experimentally measure the actual sources of aerodynamic sound. Measurement techniques such as the phased array measure the relative source strength and its frequency content at various regions in a jet. Particle Image Velocimetry (PIV) methods have been instrumental in turbulence and correlation measurements. When combined, the two techniques may establish a link between the cause and effect, i.e. turbulence and its ensuing far-field sound. However, as pointed out by Ffowcs Williams [Ref. 1] "there is no uniqueness theorem to guarantee that the source measured by any one of the several existing source location schemes is actually the origin and cause of the observed sound field." Kirchhoff's theorem shows that the same sound field could be generated by sources of different origin. In jets, our physical intuition leads us to focus on the transition region in order to link the flow unsteadiness (which is at its peak in this region) to the origin of jet noise.

In his pioneering work, Lighthill [Ref. 2] defined the equivalent sources of aerodynamic sound as the double divergence of the stress tensor $T_{ij} = \rho v_i v_j + (p - c_\infty^2 \rho)\delta_{ij} - \tau_{ij}$, where $\rho$ denotes the density, $\vec{v} = (v_1, v_2, v_3)$ is the fluid velocity, $p$ is the pressure, $c_\infty$ is the ambient sound speed, and $\tau_{ij}$ is the viscous stress tensor. In this formalism, the actual noise generating fluid is replaced with a distribution of quardrupole sources $\partial^2 T_{ij} / \partial x_i \partial x_j$ in a quiescent medium at a constant sound speed $c_\infty$. For all practical purposes, viscous stresses are considered as relatively unimportant in noise generation. Additionally when jets are isothermal, the pressure/density difference $p - c_\infty^2 \rho$ is ignored and subsequently the momentum flux $\partial^2 (\rho v_i v_j) / \partial x_i \partial x_j$ is regarded as the primary source of sound. The $U^8$ power law, which is the most quoted scaling law in aeroacoustics, is derived from Lighthill's acoustic analogy when the source is represented as the momentum flux term. It concludes that the acoustic power emitted over the surface of a large sphere surrounding a jet is proportional to the eight-power of the jet exit velocity. Lighthill's definition of the equivalent sources of aerodynamic sound has been a subject of wide spread scrutiny and interpretations – and other scaling laws have been proposed that relate the far-field sound to flow parameters such as velocity and temperature in a variety of forms.

Experimental observations by Tanna [Ref. 3] and more recent measurements by Bridges *et al*. [Ref. 4] and Viswanathan [Ref. 5] show that the effect of heat addition on jet noise depends on the jet speed. At low speeds, i.e. acoustic Mach number of 0.50 and below, heat amplifies the low to mid frequency jet noise with minimal effect at the high frequency. At high speeds (i.e. above acoustic Mach numbers of 0.90), it reduces jet noise at all frequencies. In between, e.g. at acoustic Mach number of 0.70, the heated spectrum crosses over the unheated spectrum due to enhancement of the low-frequency noise and slight weakening of the high-frequency amplitude.

These observations have compelled many researchers in the field to examine the *entropy source* term $(p - c_\infty^2 \rho)$ as a potential contributing source. For example, Morfey *et al*. [Ref. 6] offered a new two-scaling hypothesis, in favor of $U^6$ and $U^4$ power laws, and with some dependence on the mean temperature gradient. Methodical examination of jet noise data [Ref. 7, 8] reveal a more general power law $AU^n$, where the amplitude $A$ and exponent $n$ depend on

observer angle as well as jet temperature. A recent development in the utilization of scaling laws for jet mixing noise and broadband shock-associated noise in axisymmetric jets is detailed by Khavaran and Bridges [Ref. 9]

Lilley [Ref. 10] proposed a second order wave equation for the pressure fluctuations, similar to Lighthill's, but replaced $\partial(p-c_\infty^2\rho)/\partial t$ with a different expression that explicitly displays its isentropic (dipole) and non-isentropic (monopole) components. His contribution to the total acoustic power consisted of a dipole term $\partial(\rho v_i v_4)/\partial x_i$, which depends on the enthalpy gradient through $v_4 \equiv (\gamma-1)(h_\infty - h_t)$ where subscript *t* denotes a stagnation value and $\gamma$ is the specific heat ratio. In Lilley's formulation this term exhibits a $U^6$ jet noise scaling, and the monopole term is neglected.

The governing acoustic equations presented in the following section are written for axisymmetric jets, and assume a unidirectional, transversely sheared mean flow. Under such idealized conditions, the propagation equation simplifies to the second-order compressible Rayleigh operator. The resulting Green's function has a regular singular point in the vicinity of the critical layer at *r* where $1-U(r)\cos\theta/c_\infty = 0$. Goldstein [Ref. 11] describes a weakly non-parallel mean flow analysis to eliminate this singularity. Additional simplification in the source model is achieved when we consider the mean static pressure as a constant. In the final analysis two distinct space-time correlations of turbulent fluctuations in the jet need to be examined for source modeling:

Source type-1: a fourth-rank autocovariance tensor with velocity/velocity fluctuations $\overline{(v_i'v_j')_A(v_k'v_l')_B}$

Source type-2: a second-rank tensor with velocity/stagnation-enthalpy fluctuations $\overline{(v_i'h_t')_A(v_j'h_t')_B}$.

Subscripts A and B denote two points separated in space and time, and over-bar is a time-averaged value. Source type-1 is known as a momentum flux source term; while source type-2 is an enthalpy flux term. A complementary type-3 source is also present due to coupling between momentum flux and enthalpy flux terms, which is also referred to as momentum flux–enthalpy flux term. This source is a third-rank tensor $\overline{(v_j'h_t')_A(v_k'v_l')_B}$, and is generally small compared to type-2 source. An estimate of the relevance of type-3 source along the jet lip line as provided by Afsar *et al*. [Ref. 12] suggests that this source might become relatively significant compared to type-2 source at high Mach numbers. While source type-2 always makes a positive contribution to the spectrum, source type-3 is projected to make a positive contribution at high subsonic Mach numbers and a negative contribution at supersonic Mach numbers when the observer angle is close to the downstream jet axis. This latter source is tentatively ignored here and is not pursued any further.

In a RANS-based jet noise prediction approach, such as JeNo code that is used in the present computations [Ref. 13], the non-radiating background flow is usually taken to be the jet mean flow as calculated with commonly available computational fluid dynamic codes that use a Reynolds-averaged Navier-Stokes (RANS) solution with some form of a κ-ε turbulence model. The turbulent kinetic energy $\kappa = \overline{v_i'v_i'}/2$ and its dissipation rate $\varepsilon$ are sufficient to evaluate the source strength as well as its length- and time-scales in unheated jets, which are dominated by source type-1. The variance in stagnation enthalpy is an additional factor that enters the picture as a source of jet noise in heated jets (source type-2). A specialized RANS solver was discussed in a previous study [Ref. 14, 15] that predicted the variance in stagnation temperature (or enthalpy) in addition to the standard turbulence-related parameters. The approach makes use of a baseline κ-ε turbulence model with an additional two-equation scalar variance model. Determination of the scalar variance variable is achieved by selecting the appropriate mean flow quantity gradient for its production term. In jet noise the model traces the variance in stagnation temperature by choosing the gradient in total enthalpy as its production term. The Total Enthalpy Variance model is available as an option within the CARFT code [Ref. 16] and will be referred to as CRAFT-TEV. In order to achieve some level of confidence in the computational algorithm, the predicted stagnation temperature variance was compared [Ref. 17] with Rayleigh scattering measurements at a limited number of set points.

Here an Empirical Temperature Variance (ETV) model is proposed in connection with the type-2 source strength. It employs a standard RANS solvers, such as CRAFT with a standard κ-ε turbulence model [Ref. 16] or Wind-US [18, 19] to evaluate the variance in stagnation temperature. Iterations are carried out across a range of jet conditions

to fine tune empirical parameters present in the model. Subsequently the thermal source distribution as evaluated with the ETV model is compared with the computational values obtained directly from a dedicated RANS solver (CRAFT-TEV), as well as with measurements.

The remainder of this paper is organized as follows. The governing acoustic equations in the specialized case of a unidirectional parallel mean flow are discussed in section 2. In section 3 we discuss the empirical ETV model and use that to predict the intensity of thermal sources. Computational fluid dynamics solutions are presented for a host of heated subsonic jets using CRAFT-TEV solver, and the variance in total temperature is assessed against the ETV model as well as Rayleigh scattering measurements.

Section 4 presents jet noise predictions using three methods for evaluating the thermal source strength:

(i) Flow input from CRAFT code with a total enthalpy variance model (CRAFT-TEV) .

(ii) Flow input from CRAFT with a standard κ-ε model (CRAFT-κε), using ETV source model.

(iii) Flow input with Wind-US and a standard κ-ε model (Wind-κε), using ETV source model.

The latter RANS solver, i.e., Wind-US [Ref. 18, 19] is additionally used as the flow solver of choice when noise predictions are presented at a wider range of jet conditions shown in Table 2. Jet noise spectra are compared with the far-field noise measurements gathered at the Small Hot Jet Acoustic Rig (SHJAR) facility at the NASA Glenn Research Center [Ref. 20]. A summary is provided in section 5.

## 2.0 Acoustics Equations

The far-field sound spectral density at observer location $\vec{x}$, per unit volume of turbulence at source location $\vec{y}$, is (see Ref. 13, Appendix C)

$$\overline{p^2}(\vec{x},\vec{y},\omega) = \int_{\vec{\xi}}\int_{-\infty}^{+\infty} G^*(\vec{x},\vec{y}-\vec{\xi}/2,\omega)G(\vec{x},\vec{y}+\vec{\xi}/2,\omega)q(\vec{y},\vec{\xi},\tau)e^{i\omega\tau}\,d\tau d\vec{\xi}\,, \tag{1}$$

where $G$ is the Green's function (GF), and $q$ is the two-point space-time correlation between sources of turbulent mixing noise at two points A and B separated by space $\vec{\xi}$ and time $\tau$. The product of the GF and its conjugate (denoted by *) may be evaluated at the center of the correlation times a phase factor $\exp(-i\vec{k}.\vec{\xi})$, where wave number $\vec{k}$ is directed as $(\vec{x}-\vec{y})$ and has a magnitude $k=\omega/c_\infty$.

$$\overline{p^2}(\vec{x},\vec{y},\omega) = \left|G(\vec{x},\vec{y},\omega)\right|^2 \int_{\vec{\xi}}\int_{-\infty}^{+\infty} q(\vec{y},\vec{\xi},\tau)e^{i\omega\tau}e^{-i\vec{k}.\vec{\xi}}\,d\tau d\vec{\xi} \tag{2}$$

The above expression is written in a fixed frame of reference. Since the sources of jet noise are convecting downstream with a convection velocity $U_c$, the Green's function $G$ should also conform to that of a convecting singularity. As the fixed- and moving-frame source correlation functions are related $q(\vec{y},\vec{\xi},\tau)=q_m(\vec{y},\vec{\xi}_m,\tau)$, where $\vec{\xi}_m=\vec{\xi}-\hat{i}U_c\tau$, it is readily shown that

$$\int_{\vec{\xi}}\int_{-\infty}^{+\infty} q(\vec{y},\vec{\xi},\tau)e^{i\omega\tau}e^{-i\vec{k}.\vec{\xi}}\,d\tau d\vec{\xi} = \int_{\vec{\xi}_m}\int_{-\infty}^{+\infty} q_m(\vec{y},\vec{\xi}_m,\tau)e^{i\omega^s\tau}e^{-i\vec{k}.\vec{\xi}_m}\,d\tau d\vec{\xi}_m, \tag{3}$$

where source and observer frequencies are related through the Doppler factor as $\omega=\omega^s/(1-M_c\cos\theta)$. Polar angle $\theta$ is with respect to downstream axis, and $M_c=U_c/c_\infty$ is the convection Mach number for a noise-generating turbulent eddy. The convection velocity $U_c(\vec{y})$ is set equal to an appropriate weighted average of the jet exit

velocity $U_j$ and local mean velocity $U(\vec{y})$. It is noted that transformation (3) is simply an identity, and the true effect of source convection on the radiated sound is included in the GF.

The governing acoustic equation in a locally parallel mean flow (with a constant mean static pressure $\overline{p}$) is the so-called variable density inhomogeneous Pridmore-Brown equation

$$L\pi' = \Gamma, \qquad \pi' \equiv \frac{p'}{\gamma \overline{p}}, \tag{4}$$

where $L$ is a third-order wave operator

$$L \equiv D(D^2 - \frac{\partial}{\partial x_j}\widetilde{c^2}\frac{\partial}{\partial x_j}) + 2\widetilde{c^2}\frac{\partial U}{\partial x_j}\frac{\partial^2}{\partial x_1 \partial x_j}, \tag{5}$$

$D$ is a differential operator $D \equiv \partial/\partial t + U(x_2, x_3)\partial/\partial x_1$, and the sound speed is evaluated from the Favre-averaged local enthalpy $\widetilde{c^2} = (\gamma - 1)\tilde{h} = \gamma \Re \tilde{T}$. It is noted that in deriving the acoustic equation we require that both fluctuating variables and sources have a zero mean; consequently the true *equivalent* sources of aerodynamic noise are the differences between the fluctuating and Favre-averaged Reynolds stresses and enthalpy fluxes [Ref. 11]. An expanded form of source term $\Gamma$ was given in [Ref. 17], where various terms were compared for their relative significance to the noise generation. Here we adopt the following approximation

$$\Gamma \cong D\frac{\partial^2 v_i' v_j'}{\partial x_i \partial x_j} - D^2 \frac{\partial}{\partial x_j}(v_j' \frac{h_o'}{\tilde{h}}), \tag{6}$$

where $h_o' \equiv h' + v_i' v_i'/2$, and it is recognized that the divergences of both terms $\overline{\rho v_i' v_j'}$ and $\overline{\rho v_j' h_o'}$ are zero in the locally parallel mean flow approximation (or are of higher order in a slowly varying mean flow). We also replace $h_o'$ with $h_t'$, where $h_t' = h_o' - \widetilde{v_i' v_i'}/2 + \tilde{v}_i v_i'$ is the true fluctuation in stagnation enthalpy with a zero mean, $\overline{h_t'} = 0$.

When the mean flow is axisymmetric, the GF to equation (4) corresponding to a convecting singularity

$$L(Ge^{-i\omega t}) = D\left[c_\infty^2 \exp(-i\omega^s t)\delta(x_1 - U_c t)\delta(r - r^s)\right] \tag{7}$$

is given as

$$G(\vec{x}, \vec{y}, \omega) = \frac{-i}{4\pi R}\frac{(1 - M^s \cos\theta)}{(1 - M_c \cos\theta)} e^{ikR} \sum_{m=0}^{\infty} f^{(m)}(r^s, k, \theta)\cos m(\phi - \phi^s), \tag{8}$$

where superscript $s$ denotes a source location, and $f^{(m)}$ is solved numerically as a solution to the self-adjoint second-order compressible Rayleigh equation

$$\frac{d}{dr}\left[\frac{r}{\Phi^2}\frac{dg^m}{dr}\right]+\frac{r}{\Phi^2}\left[k^2(\Phi^2-\cos^2\theta)-\frac{m^2}{r^2}\right]g^{(m)}=0,\quad m=0,1,2,\cdots$$
$$\Phi^2\equiv\frac{\rho}{\rho_\infty}(1-U\cos\theta/c_\infty)^2,\quad f^{(m)}\equiv g^{(m)}(r,k,\theta)/(1-U\cos\theta/c_\infty)^3. \tag{9}$$

where $k=\omega/c_\infty$, $R$ is the far-field arc distance from jet exit, $\phi$ is the azimuthal angle in cylindrical coordinates, and $M_c=U_c/c_\infty$. The number of azimuthal modes $m$ required for a converged summation in equation (8) increases with frequency. The numerical solution to equation (9) starts with $f^{(m)}=a_m r^m$ as $r\to 0$ [Ref. 21], and continues to the jet boundary where the matching conditions are applied to determine the coefficients $a_m$.

Using the quasi-normal approximation for the joint probability distribution of turbulence [Ref. 22], the fourth-order autocovariance tensor $\overline{(v_i'v_j')_A(v_k'v_l')_B}$ is written as a product of second-order tensors. The second-order correlations may be approximated using an isotropic turbulence with separable space- and time factors. Both spatial and temporal decay factors of the correlation are well represented by exponential functions

$$f(\xi)=\exp(-\pi\xi/\ell),\quad h(\tau)=\exp(-|\tau/\tau_o|). \tag{10}$$

Here, the two-point (second-order) velocity-correlations are modeled as

$$\overline{(v_i')_A(v_j')_B}=R_{ij}(\vec{\xi}-\hat{i}U_c\tau)h(\tau) \tag{11}$$

where the spatial decay is described according to Batchelor's isotropic turbulence model [Ref . 23]

$$R_{ij}(\vec{\xi})=\overline{v_1'^2}[(f+\frac{1}{2}\xi f')\delta_{ij}-\frac{1}{2}\frac{\xi_i\xi_j}{\xi}f'],\quad f'=\partial f/\partial\xi,\quad \xi^2=\xi_1^2+\xi_2^2+\xi_3^2. \tag{12}$$

Following the *quasi-normal* assumption, the spectral density for the axial component of tensor $\overline{(v_1'v_1')_A(v_1'v_1')_B}=2\left(\overline{v_{1A}'v_{1B}'}\right)^2$ becomes

$$I_{1111}(\vec{y},\omega)=\frac{4\ell^3}{5\pi^2}\left(\overline{v_i'v_i'}\right)^2 H(\omega)N_1(k\ell);\quad H(\omega)=\int_{-\infty}^{+\infty}h^2(\tau)\exp(i\omega^s\tau)\,d\tau=\frac{\tau_o}{1+(\omega^s\tau_o/2)^2} \tag{13}$$

Turbulence length- and time-scales are calculated in the usual way from the turbulent kinetic energy and its dissipation rate as $\ell=C_\ell\kappa^{1.5}/\varepsilon$ and $\tau_o=C_\tau\kappa/\varepsilon$, and $N_1(k\ell)$ represents the source non-compactness factor that is evaluated by considering separation vector as aligned with the direction of the wave number $\vec{k}$ [Ref. 17, Appendix B]. Constants $C_\ell$ and $C_\tau$ were determined previously by calibration with unheated jet noise data when momentum flux was the only source term. These constants remain unchanged here and are used for both type-1 and type-2 sources. More elaborate source models are available in the literature that consider the turbulence as non-isotropic, and/or with multiple length-scales, or frequency-dependent length-scales. For example Leib and Goldstein [Ref. 24] proposed a non-separable axisymmetric tensor to model source type-1 space-time correlations – and used different length-scales in the stream-wise and transverse directions. Our goal at the present time is to keep the model simple

and with minimum empiricism with regard to its directionality and scales. Several assumptions were proposed in modeling the enthalpy flux correlation tensor [Ref. 17].

First, we apply the quasi-normal approximation to the autocovariance tensor for type-2 source, and express the fourth-rank tensor as a superposition of second-rank tensors. Next we assume that the coherence spectra $\gamma^2 \equiv \left|R_{vT}(f)\right|^2 / R_{vv}(f)R_{TT}(f)$ is small compared to unity, where $R_{vT}(f)$ is a Fourier transform of the two-point correlation function $R_{vT}(\tau) \equiv \overline{v_i'(t)T_t'(t+\tau)}$. Subsequently we arrive at the following

$$\overline{(v_i'h_t')_A(v_j'h_t')_B} \cong \overline{(v_i')_A(v_j')_B}\ \overline{(h_t')_A(h_t')_B} \quad . \tag{14}$$

The enthalpy correlation function is modeled using spatial and temporal functions $f(\xi)$ and $h(\tau)$ defined in equation (10)

$$\overline{(h_t')_A(h_t')_B} = \overline{(h_t')^2}\, f(\xi)h(\tau). \tag{15}$$

Following the steps outlined in [Ref. 17], the spectral density for the two source terms in equation (6) may be expressed as

$$\overline{p^2}(\vec{x},\vec{y},\omega) = \frac{\rho_\infty^2 I_{1111}(\vec{y},\omega)k^4(1-U\cos\theta/c_\infty)^2(\cos^2\theta+Q\sin\theta)^2}{(4\pi R)^2(1-M_c\cos\theta)^2} \times \left[\begin{array}{c} A(\cos^2\theta+Q\sin\theta)^2 \\ +B(1-U\cos\theta/c_\infty)^2\dfrac{15}{16}\dfrac{c_\infty^2}{\kappa}\dfrac{\overline{h_t'^2}}{\tilde{h}^2} \end{array}\right] \sum_{m=0}^{\infty}(1+\delta_{m0})f^{(m)}f^{*(m)} \tag{16}$$

where $Q^2 \equiv (\rho/\rho_\infty)(1-U\cos\theta/c_\infty)^2 - \cos^2\theta$. Constants *A* and *B* are determined by calibrating with jet noise data.

## 3.0 Subsonic Flowfield Simulations

A set of eight subsonic jets within the Tanna matrix [Ref. 25] is listed in Table 1. A 2-inch (5.08cm) diameter convergent nozzle was considered for flow simulation and jet noise prediction. This set was also examined in a previous study [Ref. 17] for flow simulation with the CRAFT-TEV model. Here we present some of the earlier computations using CRAFT-TEV solver with an emphasis on the distribution of the temperature variance in the jet and comparison with data obtained with a Rayleigh scattering technique [Ref. 26, 27]. We also examine an empirical temperature variance (ETV) model that evaluates the total temperature variance using a function of mean stagnation temperature in the flow. A more comprehensive set of subsonic conditions will be considered later on at the conditions of Table 2 as we implement the ETV model in conjunction with the Wind-κε RANS solver [Ref. 18].

Each set point (sp) in Table 1 identifies a jet at a nozzle plenum pressure ratio (NPR), stagnation temperature ratio $T_t/T_\infty$, exit static temperature ratio $T_j/T_\infty$, aerodynamic Mach number $M_j = U_j/c_j$, and acoustic Mach number $M_a = U_j/c_\infty$. These conditions have been studied extensively in the past using the CRAFT-κε RANS solver [Ref. 16] to predict turbulence in the transition region where most of the jet noise is produced. Comparisons were made previously with available PIV data collected at SHJAR facility [Ref. 4, 20]. Simulations with the CRAFT code use a 316x171 computational grid, which includes the internal nozzle region well upstream of the exit plane. The computational domain extends 50 jet diameters in the streamwise direction from the nozzle exit, and 12.5 diameters

in the radial direction, sufficiently distant to minimize boundary condition placement impact on the shear layer entrainment path-lines. Nozzle flow boundary conditions were prescribed uniformly as inflow stagnation conditions for pressure and temperature imposed well upstream of the nozzle exit. The predicted centerline decay of mean axial velocity and turbulent kinetic energy were presented in [Ref. 17] as a function of Witze's similarity parameter and will not be repeated here.

## 3.1 An Empirical Temperature Variance (ETV) Source Model

The thermal source strength, see second term in equation (16), is proportional to $\overline{h_t'^2}/\tilde{h}^2$. We intend for the ETV source strength $S_T$ to resemble $\langle h_t' \rangle / \tilde{h}$ in its distribution, and to approach zero under unheated jet conditions $T_t / T_\infty \to 1$.

We define

$$S_T = \left( \left| \frac{dT_t}{dr} \right| \frac{D_j}{T_\infty} \right)^{\alpha} \frac{(1 - 1/NTR)^{\delta}}{6} \beta \,,$$

where

$$\beta = \begin{cases} \beta_o + (1-\beta_o)\, x_1 / L_c \,, & x_1 / L_c \le 1 \\ 1 \qquad\qquad\qquad\quad \,, & x_1 / L_c > 1 \end{cases} \tag{17}$$

$$\alpha = 0.20, \quad \beta_o = 0.70, \quad \delta = 1 + 1/(3\,NPR)$$

Axial distance $x_1$ is measured from the jet exit, and $L_c$ is the length of the potential core in the jet. For example, Witze's axial similarity parameter $x_w$ in subsonic jets may be used to evaluate $L_c$ [Ref.28]

$$x_W = 0.08\left( \sqrt{\rho_\infty / \rho_j} - 0.16 U_j / c_\infty \right) (\rho_\infty / \rho_j)^{-0.22} x_1 \,. \tag{18}$$

Parameters *NTR* and *NPR* in equation (17) denote the jet plenum temperature ratio and pressure ratio, respectively.

Sample RANS predictions with CRAFT-TEV and comparison with the Rayleigh scattering measurements are shown in figures 1 to 4. The non-intrusive molecular Rayleigh scattering technique [Ref. 26, 27] is used to measure jet velocity, static temperature and density simultaneously at a sampling rate of 10 kHz, and the root-mean-square (rms) in total temperature fluctuations $< T_t' >$, is obtained as the variance in $(T + v_1^2 / 2c_p)$. Measurements and predictions are presented separately, as parts (a) and (b), in order to avoid overcrowded figures. Figures 5 to 8 show the axial turbulent velocity component $(u'/U_j)$ at indicated streamwise locations as measured with the Rayleigh scattering methods. Part (b) in each figure shows a comparison with CRAFT predictions assuming $\overline{u'^2} = 2\kappa / 3$. Although the centerline values near the jet exit appear less agreeable in several cases, nonetheless the experimental data agree qualitatively with the computational results in their peak values as well as radial profiles. Thermal fluctuations, in general, display a distribution similar to that of the turbulent kinetic energy.

Figures 9 to 15 show computational results for the square root of the normalized turbulent kinetic energy $\kappa^{0.50} / U_j$ and enthalpy source strength $< T_t' > / \tilde{T}$ (or equivalently $\langle h_t' \rangle / \tilde{h}$) at conditions of Table 1. A third contour plot displays the ETV source strength $S_T$ using input CRAFT-κε. The empirical temperature variance model shows a source distribution similar to CRAFT-TEV, although small differences in intensity level are noticeable at several

conditions. The source strength is practically insignificant at unheated conditions of sp03 (Figure 15) and sp07 (not shown here). We use both ETV model and CRAFT-TEV in our noise predictions later on, and show that the two results agree to within the experimental uncertainty in noise measurements.

**Table 1. Tanna Matrix Set Point Conditions**

| sp | NPR | $T_t/T_\infty$ | $T_j/T_\infty$ | $M_a$ | $M_j$ |
|---|---|---|---|---|---|
| 03 | 1.197 | 1.000 | 0.950 | 0.50 | 0.51 |
| 23 | 1.103 | 1.810 | 1.760 | 0.50 | 0.37 |
| 42 | 1.066 | 2.750 | 2.700 | 0.50 | 0.30 |
| 07 | 1.861 | 1.000 | 0.840 | 0.90 | 0.98 |
| 27 | 1.361 | 1.922 | 1.760 | 0.90 | 0.68 |
| 46 | 1.225 | 2.861 | 2.700 | 0.90 | 0.54 |
| 29 | 1.890 | 2.114 | 1.760 | 1.33 | 1.00 |
| 49 | 1.692 | 3.138 | 2.700 | 1.48 | 0.90 |

## 4.0 Acoustic Results

Noise predictions are carried out according to equation (16) with the correlation coefficient $I_{1111}$ defined in equation (13). A RANS flow solver provides the mean flow as well as the turbulent kinetic energy $\kappa$ and dissipation rate $\varepsilon$, which are necessary in evaluating source type-1. Source type-2 is evaluated using either a dedicated RANS solver (CRAFT-TEV), or a standard RANS solver combined with the ETV model described in equation (17). Jet noise spectra are evaluated as a constructive contribution from the two source types, and are presented as lossless at arc distance $R/D_j = 100$. Acoustic results are displayed as the sound spectral density per Strouhal number (SPD-dB) vs. Strouhal frequency (St) where

$$SPD \equiv 10 Log\left(p^2 U_j / P_{ref}^2 D_j\right), \qquad St = f D_j / U_j \ . \tag{19}$$

### 4.1 Enthalpy Source Noise

Spectral predictions are carried out at the subsonic jet conditions listed in Table 1 using two different flow solvers and three methods for computing thermal source strength as described in section 1. Jet noise predictions are compared with narrow-band spectral measurements gathered at the SHJAR facility at the NASA Glenn Research Center [Ref. 4, 20].

Intensities for type-1 and type-2 sources were examined earlier in figures 9 through 15. The predicted sound spectral density is shown at three inlet angles of 90°, 120°, and 150° in figures 16, 17 and 18. Computations were carried out with RANS input from CRAFT code, and with the type-2 source evaluated according to; (i) empirical model (ETV); (ii) CRAFT-TEV model. Figure 16 corresponds to two unheated jets at set points sp03 and sp07. Figure 17 shows three jets at a common exit static temperature ratio of 1.76 and at acoustic Mach numbers of 0.50, 0.90, and 1.33. Similarly, figure 18 corresponds to jets at a common static temperature ratio of 2.70 and at acoustic Mach numbers of 0.50, 0.90, and 1.48. In general the two predictions are in close agreement. This indicates that the empirical model is a viable substitute for type-2 source strength; at least at jet conditions examined here, and could replace the enthalpy variance model available in CRAFT-TEV code as an alternative means of evaluating $\langle h_t' \rangle / \tilde{h}$ source strength. The two spectral predictions coincide at unheated conditions due to insignificant contributions from

type-2 source (Fig. 16). Overall, the computations are in close agreement with measurements. The major discrepancy arises at high speeds, i.e. at set points sp29 and sp49 (figures 17c and 18c), where the predicted high frequency noise attenuates faster than measurements and lacks a broadening at the peak that is commonly measured at aft angles in heated jets. This feature is particularly visible at set point sp49 at $150^o$. The parallel flow approximation is known to exaggerate the attenuation of the high frequency noise, and to generate a fairly larger cone of silence compared to a spreading jet. Scattering of the high frequency jet noise from the nozzle lip could also be another mechanism contributing to the near-axis jet noise. The extension/broadening of the spectrum-peak and the appearance of a second peak at a relatively higher frequency is a recurrent feature observed in supersonic jet noise measurements.

Next we examine the impact of the flow solver on the predicted noise with a third set of computations that use Wind-US [Ref. 18] RANS solver. Since Wind code is not currently outfitted with the enthalpy variance and dissipation rate model, the type-2 source strength was evaluated with the ETV model, while type-1 source strength uses a $\kappa$-$\varepsilon$ turbulence model. Figures 19 to 24 present the source distributions for each source type at heated conditions considered above, and should be compared with similar results using CRAFT solver presented in figures 9 to 14. Although the two flow solvers do not provide identical results, the overall source distributions and intensity levels remain in close agreement. Subsequent jet noise predictions that use the empirical ETV model with both Wind-$\kappa\varepsilon$ and CRAFT-$\kappa\varepsilon$ input are also shown in figures 25, 26 and 27 while calibration constants in evaluating the time- and length-scales remained unchanged. The two sets of spectra are practically similar and slight differences in the flow solvers have inconsequential impact on the predicted jet noise.

## 4.2 Model Source Validation – A Comprehensive Set of Subsonic Conditions

Here we set out to examine the source model proposed in section 3 under a wider range of subsonic jet conditions listed in Table 2. Twenty set points are divided into four distinct categories – the first three groups are at acoustic Mach numbers of 0.50, 0.70, and 0.90 respectively, with five jets listed within each group in the order of increasing temperature. Jets in the fourth group are at Mach number 1.0, i.e. nozzle pressure ratio of 1.89, and with a plenum temperature ratio in the order from 1.0 to 3.20. The nozzle of interest in is the 2-inch diameter convergent nozzle smc000 studied extensively for aerodynamic performance and jet noise at the SHJAR facility [Ref. 29, 30]. Acoustic data repeatability has been determined to be within 0.50 dB in one-third-octave band at all frequencies. Mean flow and turbulence calculations were performed with the Wind-US code using a $\kappa$-$\varepsilon$ turbulence model. Subsequent noise predictions were carried out using type-1 and type-2 sources, with the enthalpy-related source evaluated according to the empirical ETV model discussed in section 3.

As before, spectral predictions are presented as lossless and are compared with the narrow-band SHJAR noise measurements at two inlet angles of $90^o$ and $150^o$ at an arc distance of $100D_j$. These results are shown in 20 separate figures, from 28 through 47, where each jet is identified through a *Reading No.* as listed in column-2,Table 2. Reasonably accurate jet noise spectra were predicted at all subsonic exhaust-speeds as seen in figures 28 through 43. Shortfalls develop at aft angles and at supersonic exhaust speeds at the latter four conditions in Table 2. These

**Table 2. Subsonic Set Point Conditions**

| sp | Reading | NPR | $T_t / T_\infty$ | $T_j / T_\infty$ | $M_a$ | $M_j$ |
|---|---|---|---|---|---|---|
| 3 | 1513 | 1.188 | 1.040 | 0.95 | 0.50 | 0.502 |
| 8 | 1521 | 1.188 | 1.047 | 1.00 | 0.50 | 0.501 |
| 163 | 1525 | 1.168 | 1.154 | 1.10 | 0.50 | 0.476 |
| 153 | 1528 | 1.153 | 1.251 | 1.20 | 0.50 | 0.456 |
| 15 | 1531 | 1.128 | 1.479 | 1.43 | 0.50 | 0.419 |
| 5 | 1514 | 1.418 | 1.025 | 0.90 | 0.70 | 0.724 |
| 10 | 1523 | 1.389 | 1.100 | 1.00 | 0.70 | 0.702 |
| 165 | 1526 | 1.346 | 1.200 | 1.10 | 0.70 | 0.666 |
| 155 | 1529 | 1.318 | 1.300 | 1.20 | 0.70 | 0.640 |
| 17 | 1532 | 1.26 | 1.530 | 1.43 | 0.70 | 0.585 |
| 7 | 1515 | 1.834 | 1.017 | 0.85 | 0.90 | 0.972 |
| 12 | 1524 | 1.694 | 1.164 | 1.00 | 0.90 | 0.900 |
| 167 | 1527 | 1.616 | 1.260 | 1.10 | 0.90 | 0.857 |
| 157 | 1530 | 1.563 | 1.359 | 1.20 | 0.90 | 0.825 |
| 19 | 1533 | 1.452 | 1.592 | 1.43 | 0.90 | 0.751 |
| 405 | 1614 | 1.893 | 1.00 | 0.83 | 0.910 | 1.000 |
| 415 | 1584 | 1.893 | 1.800 | 1.50 | 1.224 | 1.000 |
| 425 | 1572 | 1.893 | 2.200 | 1.83 | 1.356 | 1.000 |
| 435 | 1565 | 1.893 | 2.700 | 2.26 | 1.500 | 1.000 |
| 445 | 1554 | 1.893 | 3.200 | 2.70 | 1.630 | 1.000 |

results, presented in figures 44 to 47, show that both the spectral peak and its amplitude at the aft angle of 150$^o$ fall short of measurements under supersonic conditions. This discrepancy, noted to increase at higher exhaust temperature (velocity), was also discussed earlier in the context of supersonic conditions in Table 1. The broadening of the spectrum peak at 150$^o$ with increasing jet temperature is quite noticeable in the data – and in fact a second spectral peak at the Strouhal frequency of ~ 0.30 can clearly be distinguished at acoustic Mach numbers of 1.50 and 1.63 in figures 46 and 47. As pointed out earlier, we attribute this shortcoming to the overemphasized refraction phenomena in a parallel mean flow approximation. As for our primary goal, the empirical ETV source model (i.e. type-2 source) appears to have worked successfully as a replacement for the variance of thermal fluctuations as calculated with a dedicated flow solver. This model, described in equation (17), depends entirely on the mean flow parameters and may readily be implemented with input from a standard flow solver.

## 5.0 Summary

In this study we presented a model for the enthalpy flux source term (i.e. type-2 source) within the framework of the generalized Acoustic Analogy. The main parameter of interest was the variance in the jet stagnation enthalpy. The goal was to conceive a more practical computational approach in connection with type-2 source strength that would be independent of a dedicated RANS solver. Following the representation outlined in equation (17), the strength of the enthalpy-related source was evaluated from readily available mean flow parameters supplied by the standard RANS solvers. The model was subsequently used to evaluate an approximate form of the velocity/stagnation-enthalpy autocovariance tensor in the context of a physics-based jet noise modeling approach. The spectral computations were carried out with the help of jet noise prediction code "JeNo" according to equation (16), and with the propagation Green's function evaluated following equation (9). The major

simplification in the computations is associated with the parallel flow approximation. We argued that this assumption leads to a larger than measured cone of silence near the downstream jet axis at supersonic exhaust speeds. We also chose to tentatively ignore the type-3 source, i.e. momentum-flux enthalpy-flux coupling term, due to its small contribution to jet noise at subsonic Mach numbers. Predicted spectra were in reasonably good agreement with measurements at all subsonic speeds considered in Tables 1 and 2. At supersonic exhaust speeds, however, the predicted spectra missed some commonly observed features at aft angles such as spectral-peak broadening, and/or the appearance of a second peak at a relatively higher frequency. We attributed this shortcoming to the overemphasized refraction phenomena in a parallel mean flow approximation. Computation of the Green's function in a spreading jet may be carried out by solving a vector Green's function in a set of five linear equations that govern the non-radiating base flow in the acoustic equations [Ref. 11]. These computations become very intensive and should preferably be carried out with the adjoint form of the governing equations.

## References


[1] Ffowcs Williams, J. E., "Noise mechanisms, technical evaluation report," *AGARD-CP-131*, (1974), pp. vii-xx.
[2] Lighthill, M. J., "On sound generated aerodynamically: I. general theory," Proceedings R. Soc. London, **A211**, (1952), pp. 564-587.
[3] Tanna, H.K., "The influence of temperature on shock-free supersonic jet noise," J. Sound Vib., **39(4),** (1975), pp. 429-460.
[4] Bridges, J., and Wernet, M. P., "Measurements of the aeroacoustic sound source in hot jets," AIAA-2003-3130, May 2003.
[5] Viswanathan, K., "Aeroacoustics of hot jets," J. Fluid Mechanics, **519**, (2004), pp. 39-82.
[6] Morfey, C. L., and Szewczyk, V. M., "New scaling laws for hot and cold jet mixing noise based on a geometric acoustic model," J. Sound Vib., **61(2)**, (1978), pp. 255-292.
[7] Tam, C. K.W., "Dimensional analysis of jet noise data," AIAA Journal, **44(3)**, (2006), pp. 512-522.
[8] Viswanathan, K., "Scaling laws and a method for identifying components of jet noise," AIAA Journal, **44(10)**, (2006), pp. 2272-2285.
[9] Khavaran, A., and Bridges, J., "Development of jet noise power spectral laws using SHJAR data," AIAA-2009-3378, May 2009.
[10] Lilley, G. M., "The radiated noise from isotropic turbulence with application to the theory of jet noise," J. Sound Vib., **190(3)**, (1996), pp. 463-476.
[11] Goldstein, M. E., and Leib, S. J., "The aeroacoustics of slowly diverging supersonic jets," J. Fluid Mechanics, **600**, (2008), pp. 291-337.
[12] Afsar, M. Z., Goldstein, M. E., and Fagan, A. "The influence of enthalpy flux – momentum flux coupling on the acoustic spectrum of heated jets," AIAA-2011-1033, January 2011.
[13] Khavaran, A., Bridges, J., and Georgiadis, N., "Prediction of turbulence-generated noise in unheated jets," Part 1: JeNo Technical Manual, NASATM-2005-213827, 2005.
[14] Nagano, Y. and Kim. C., "A Two-Equation Model for Heat Transport in Wall Turbulent Shear Flows," J. Heat Transfer **(110)**, (1988), pp. 583-589.
[15] Kenzakowski, D.C., "RANS modeling improvements for jets using scalar variance equations," AIAA-2006-0491, 2006.
[16] Dash, S.M., Kenzakowski, D.C., Seiner, J.M., and Bhat, T.R.S., "Recent advances in jet flowfield simulation: Part I - Steady flows," AIAA 93-4390, 15th AIAA Aeroacoustics Conf., Oct. 25-27, 1993.
[17] Khavaran, A., Kenzakowski, D. C., and Mielke-Fagan, A. F., "Hot jets and sources of jet noise," International J. Aeroacoustics, **9(4,5)**, 2010, pp. 491-532.
[18] Nelson, C.C., "An overview of the NPARC alliance's Wind-US flow solver," AIAA-2010-27, Jan. 2010.
[19] Georgiadis, N.J., Yoder, D.A., and Engblom, W.A., "Evaluation of modified two-equation turbulence models for jet flow predictions," *AIAA Journal*, **44(12)**, (2006), pp. 3107-3114.
[20] Bridges, J., "Effect of heat on space-time correlation in jets," AIAA-2006-2534, May 2006.
[21] Tam, C. K. W., and Auriault, L. "Mean flow refraction effects on sound radiated from a localized source in jets," J. Fluid Mechanics, **370**, (1999), pp. 149-174,
[22] Monin, A. S., and Yaglom, A. M., *Statistical Fluid Mechanics: Mechanics of Turbulence*, vol. 2, MIT Press, 1975.
[23] Batchelor, G. K., *The Theory of Homogeneous Turbulence*, Cambridge University Press, Cambridge, 1960.
[24] Leib, S. J., and Goldstein, M. E., "Hybrid source model for predicting high-speed jet noise," AIAA Journal, **49(7),** (2011), pp. 1324-1335.
[25] Tanna, H. K., "An experimental study of jet noise, part I: turbulent mixing noise," J. Sound Vib., **50(3)**, (1977), pp. 405-428.
[26] Mielke, A. F., Elam, K. A., and Sung, C. J., "Molecular Rayleigh scattering diagnostic for dynamic temperature, velocity, and density measurements," AIAA-2006-2969, 2006.
[27] Mielke, A. F., Elam, K. A., and Sung, C. J., "Time-Resolved Rayleigh scattering measurements in hot gas flows," AIAA-2008-262, 2008.
[28] Witze, P. O., "Centerline velocity decay of compressible free jets," AIAA Journal, 12(4), (1974), pp. 417-418.
[29] Brown, C. A., and Bridges, J., "Small Hot Jet Acoustic Rig validation," NASA TM – 2006-214234, 2006.
[30] Bridges, J., and Wernet, M. P., "Effect of temperature on jet velocity spectra," AIAA-2007-3628, 2007.

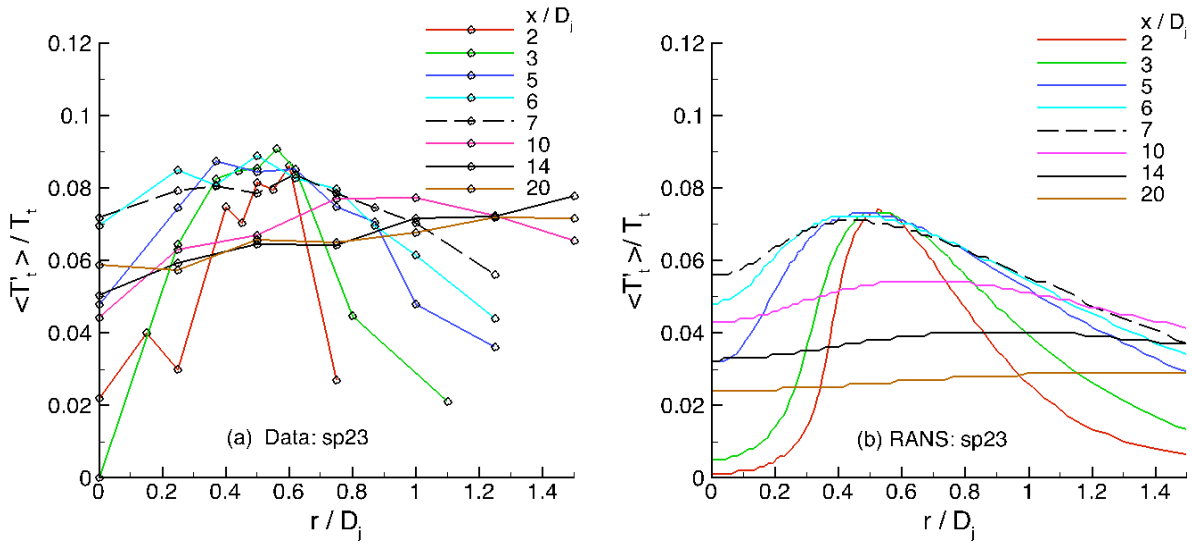


**Figure 1.** **Variance in total temperature at set point sp23, Table 1: (a) Rayleigh scattering measurements; (b) predictions with CRAFT-TEV flow solver.**

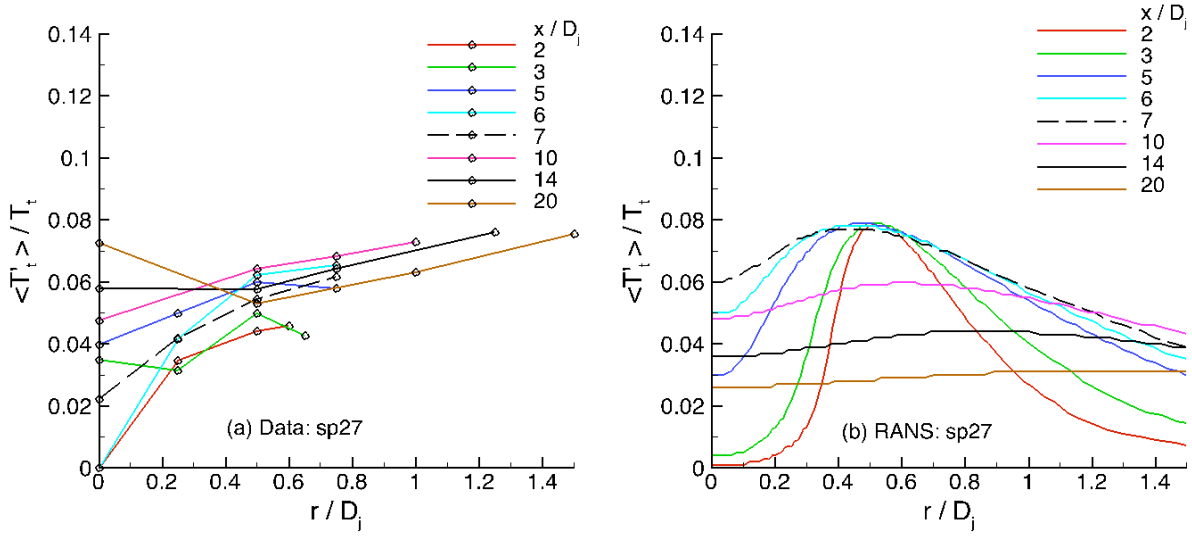


**Figure 2.** **Variance in total temperature at set point sp27, Table 1: (a) Rayleigh scattering measurements; (b) predictions with CRAFT-TEV flow solver.**

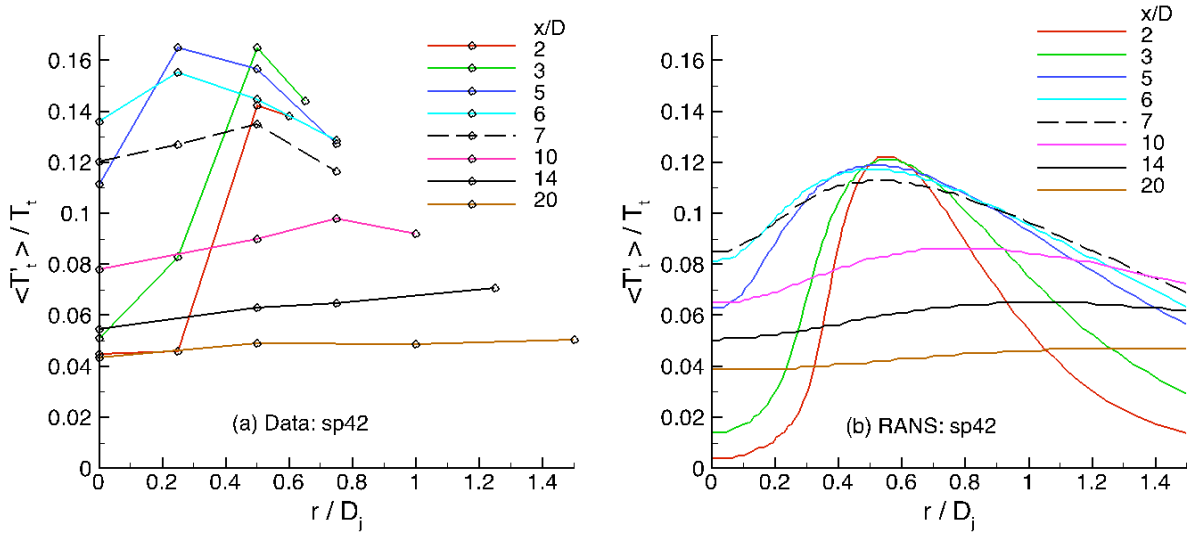


**Figure 3.** **Variance in total temperature at set point sp42, Table 1: (a) Rayleigh scattering measurements; (b) predictions with CRAFT-TEV flow solver.**

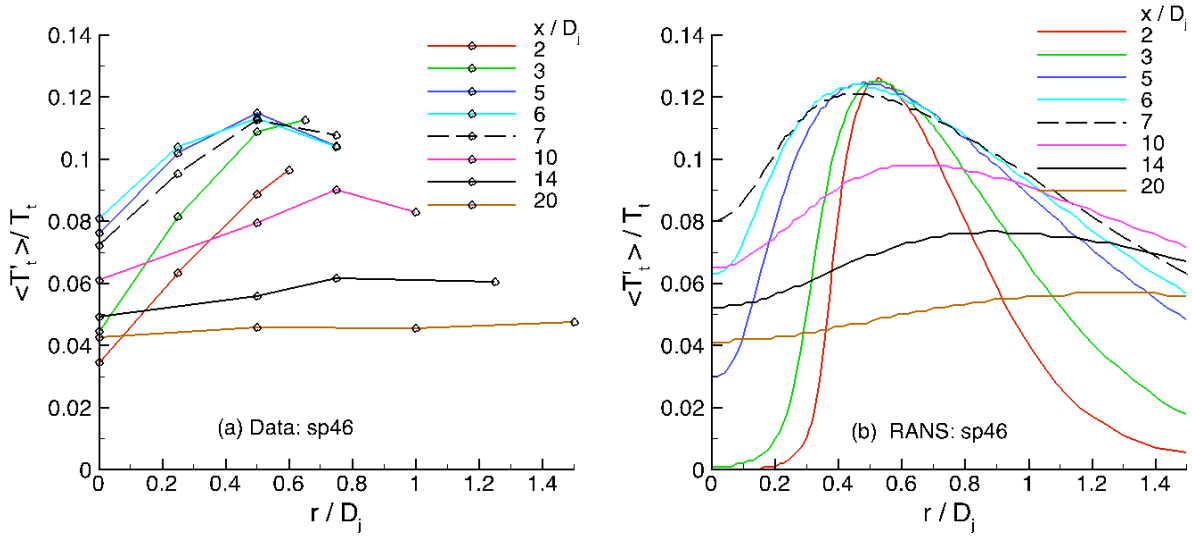


**Figure 4.** **Variance in total temperature at set point sp46, Table 1: (a) Rayleigh scattering measurements; (b) predictions with CRAFT-TEV flow solver.**

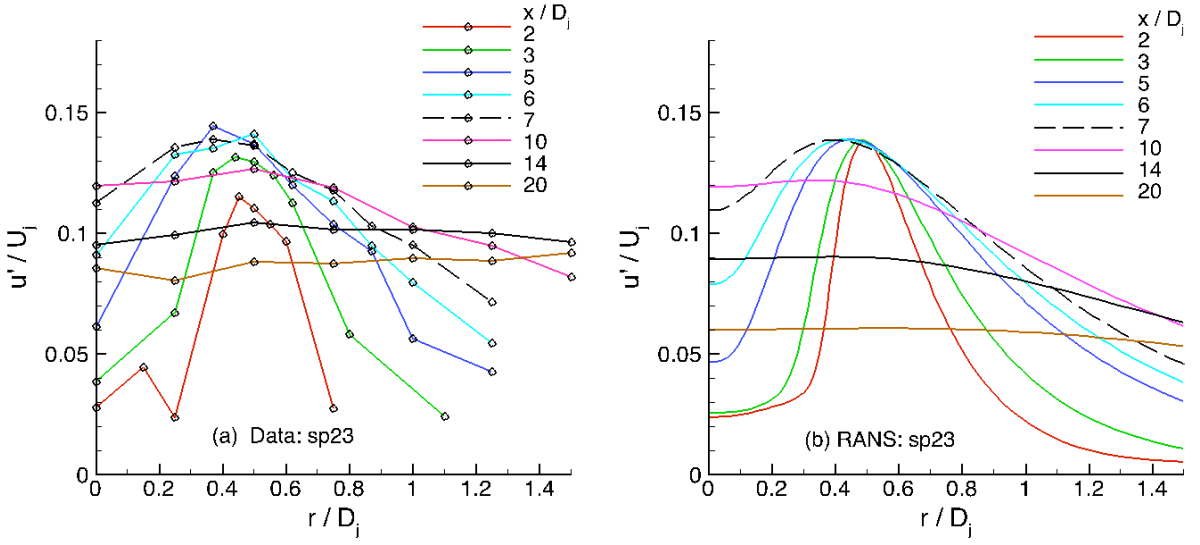


**Figure 5.** **Streamwise turbulent velocity component (rms) at indicated axial locations at set point sp23 from Table 1: (a) Rayleigh scattering data; (b) CRAFT RANS predictions.**

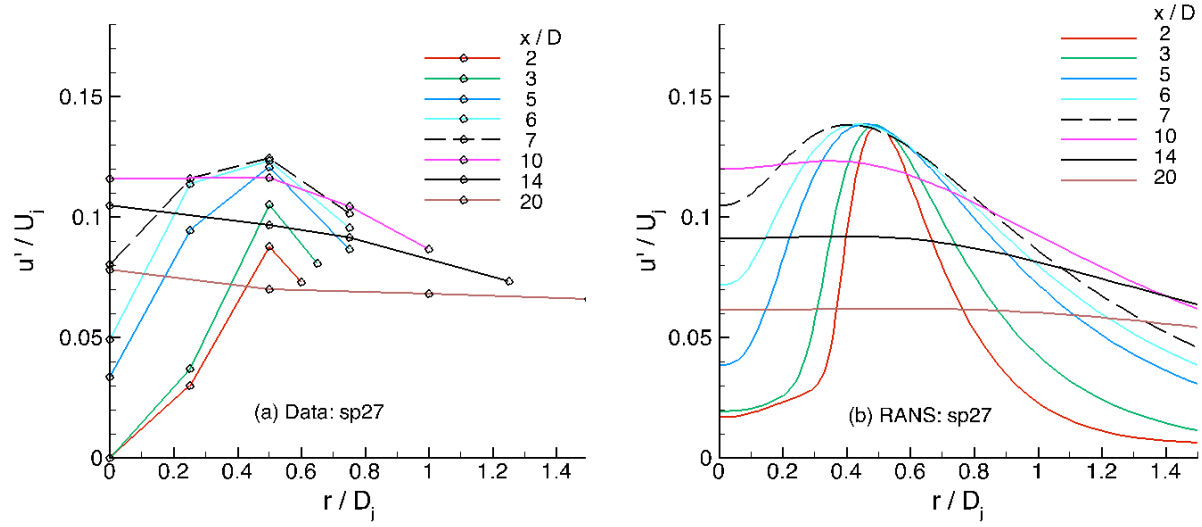


**Figure 6.** **Streamwise turbulent velocity component (rms) at indicated axial locations at set point sp27 from Table 1: (a) Rayleigh scattering data; (b) CRAFT RANS predictions.**

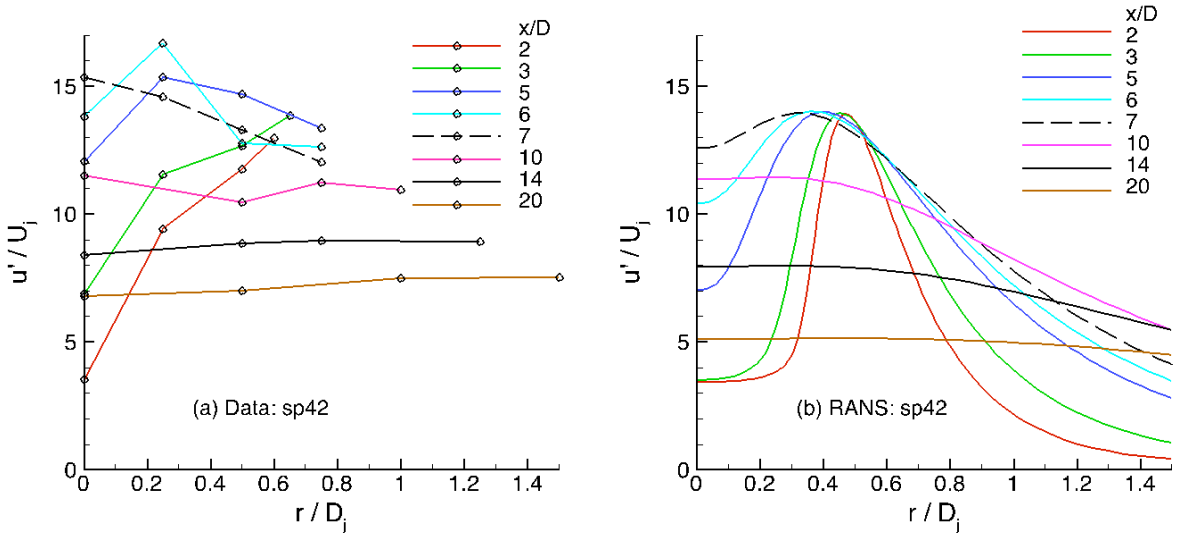


**Figure 7. Streamwise turbulent velocity component (rms) at indicated axial locations at set point sp42 from Table 1: (a) Rayleigh scattering data; (b) CRAFT RANS predictions.**

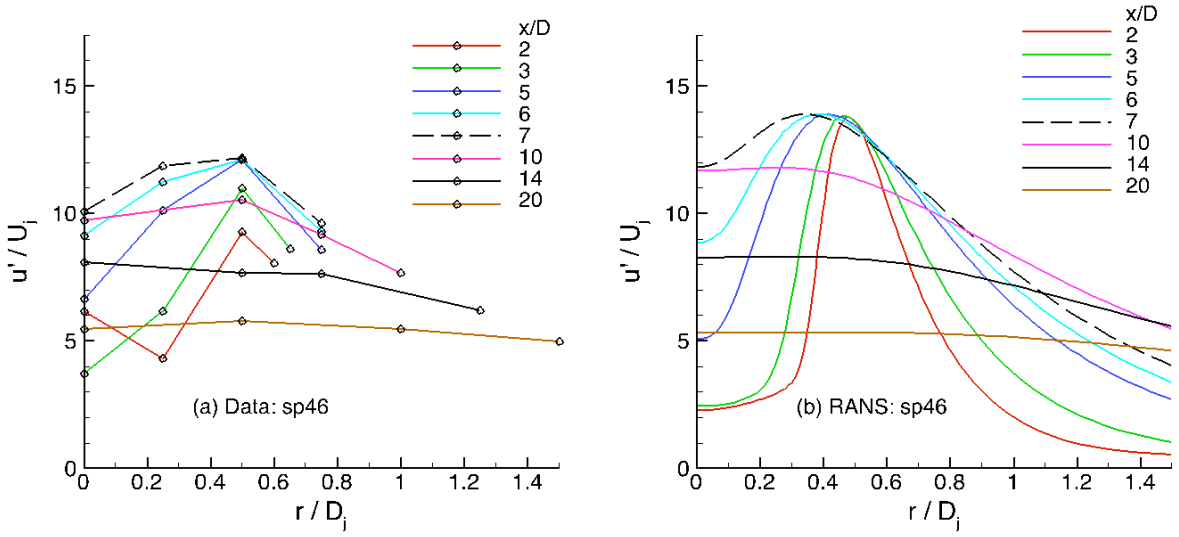


**Figure 8. Streamwise turbulent velocity component (rms) at indicated axial locations at set point sp46 from Table 1: (a) Rayleigh scattering data; (b) CRAFT RANS predictions.**

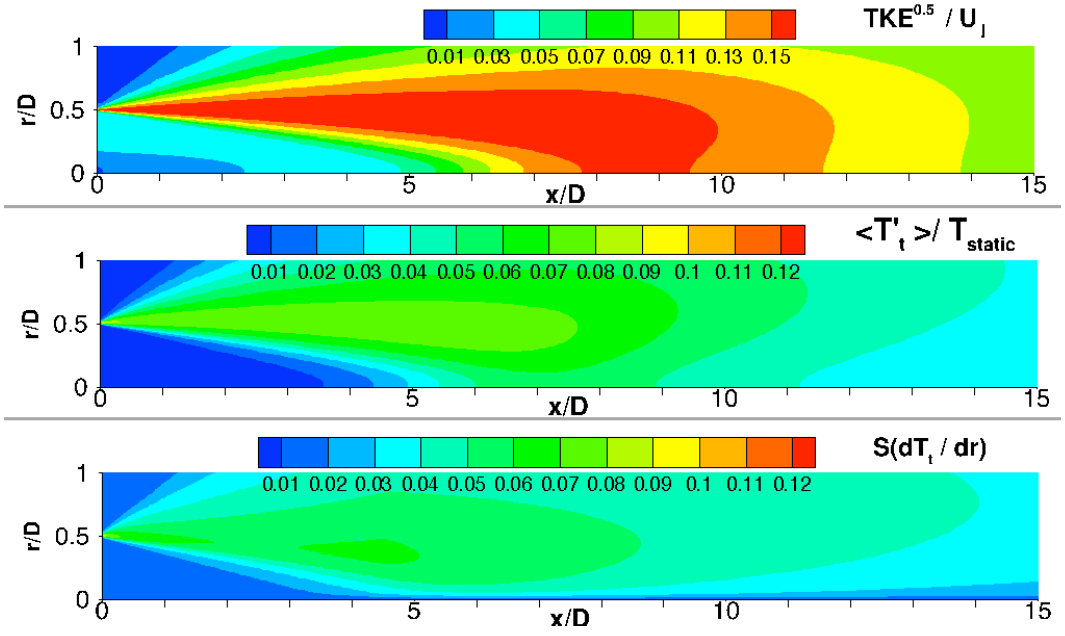


**Figure 9.** **CRAFT RANS predictions for turbulent kinetic energy (top) and variance in stagnation temperature (middle) in the jet at set point sp23 shown in Table 1. The ETV source strength with CRAFT input is shown in the bottom.**

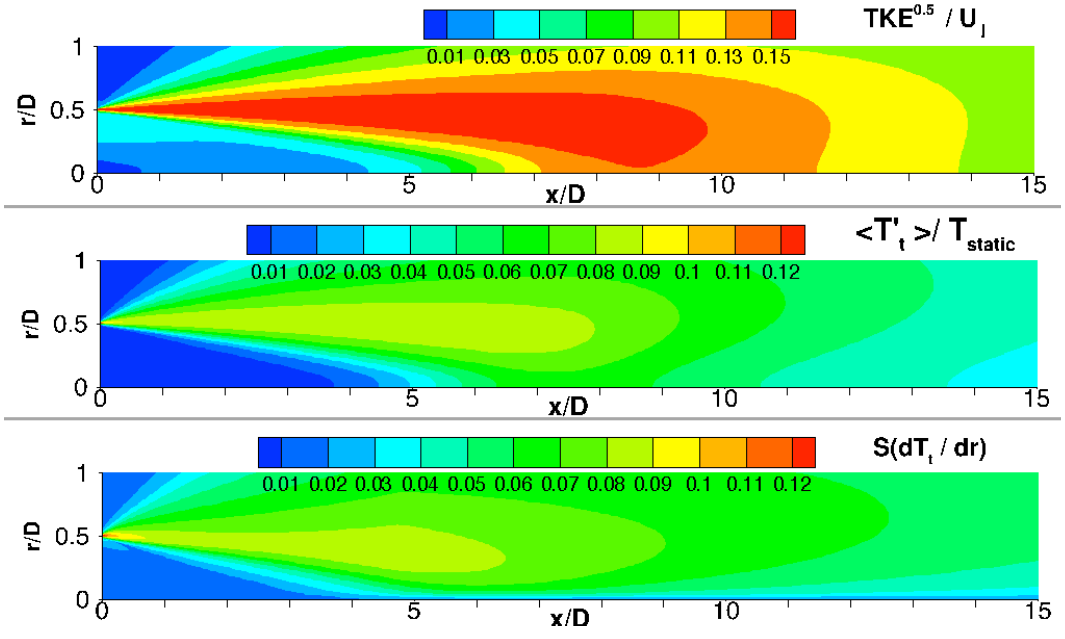


**Figure 10.** **CRAFT RANS predictions for turbulent kinetic energy (top) and variance in stagnation temperature (middle) in the jet at set point sp27 shown in Table 1. The ETV source strength with CRAFT input is shown in the bottom.**

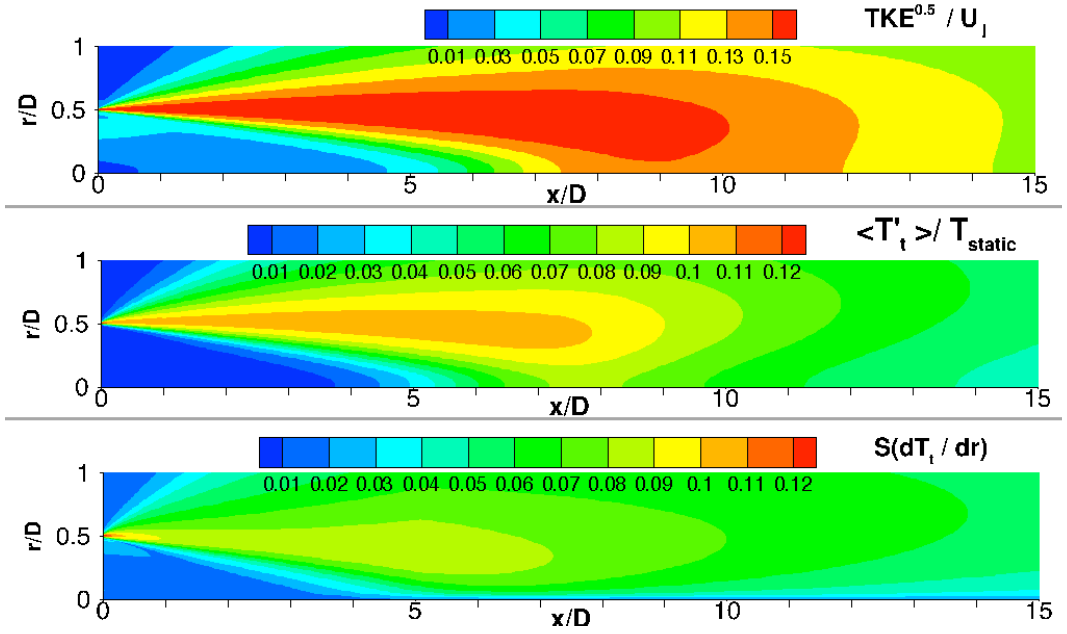


**Figure 11.** **CRAFT RANS predictions for turbulent kinetic energy (top) and variance in stagnation temperature (middle) in the jet at set point sp29 shown in Table 1. The ETV source strength with CRAFT input is shown in the bottom.**

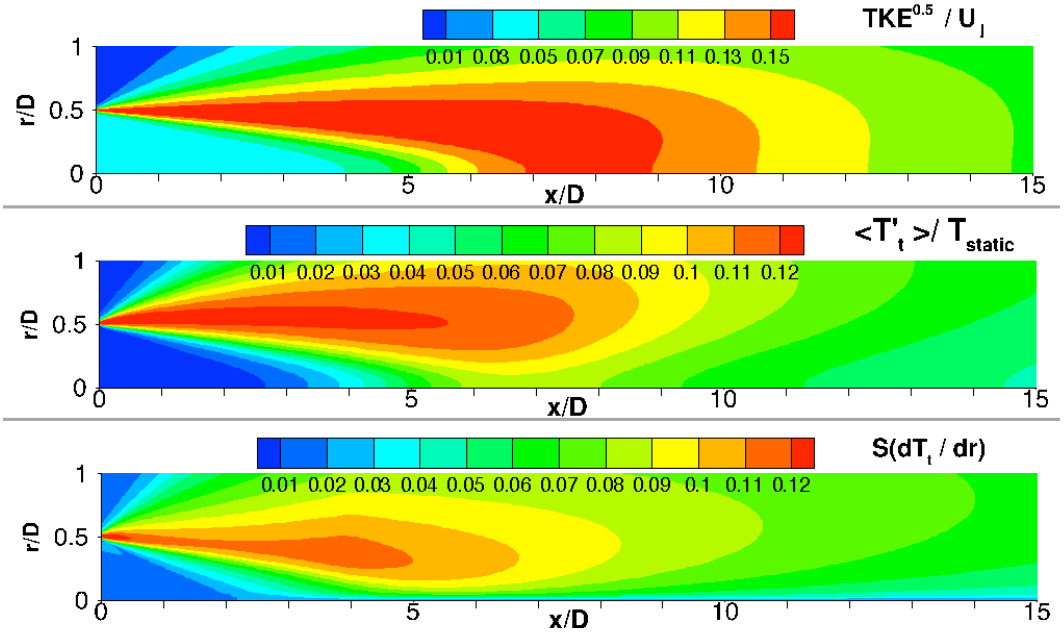


**Figure 12.** **CRAFT RANS predictions for turbulent kinetic energy (top) and variance in stagnation temperature (middle) in the jet at set point sp42 shown in Table 1. The ETV source strength with CRAFT input is shown in the bottom.**

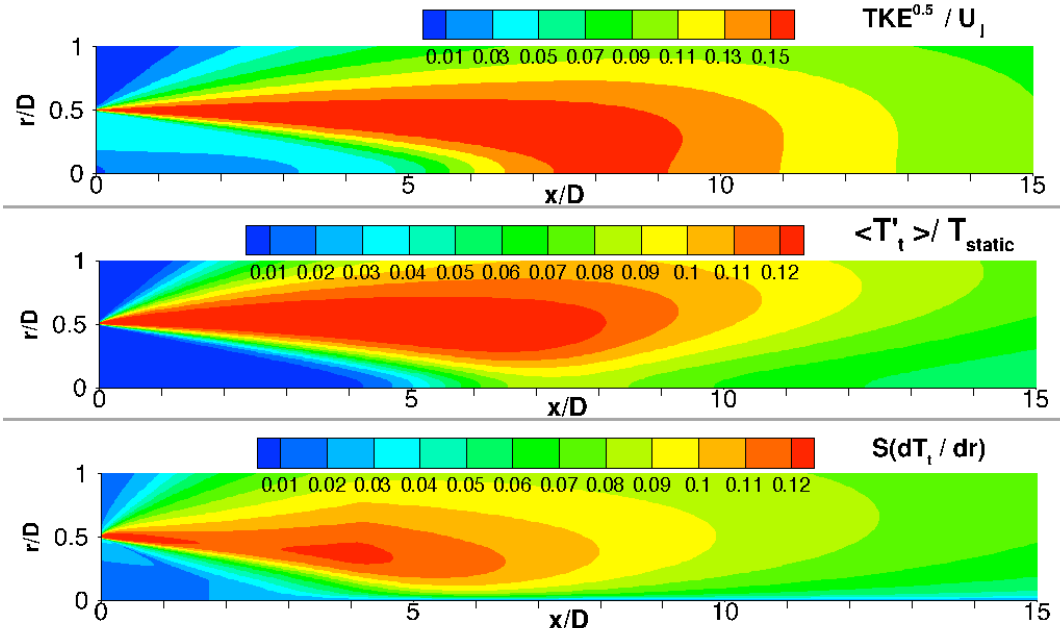


**Figure 13.** **CRAFT RANS predictions for turbulent kinetic energy (top) and variance in stagnation temperature (middle) in the jet at set point sp46 shown in Table 1. The ETV source strength with CRAFT input is shown in the bottom.**

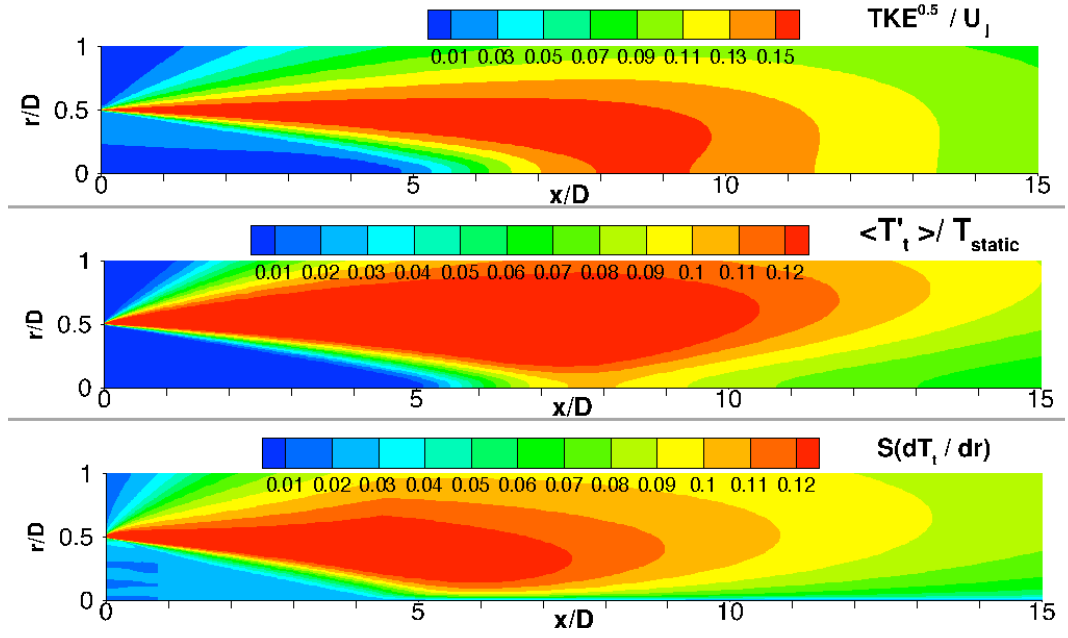


**Figure 14.** **CRAFT RANS predictions for turbulent kinetic energy (top) and variance in stagnation temperature (middle) in the jet at set point sp49 shown in Table 1. The ETV source strength with CRAFT input is shown in the bottom.**

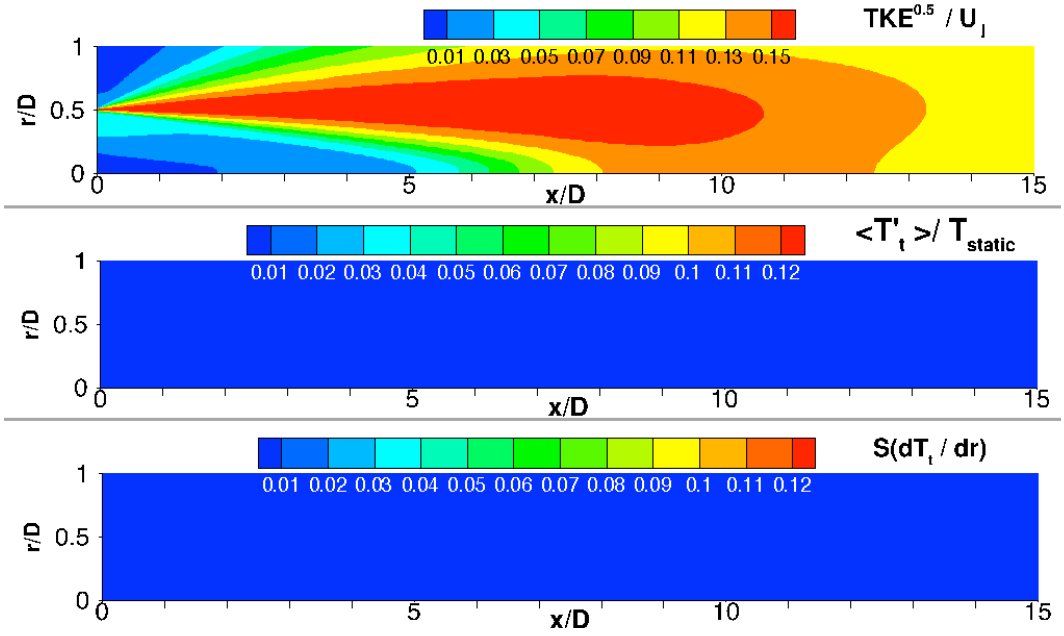


**Figure 15.** **CRAFT RANS predictions for turbulent kinetic energy (top) and variance in stagnation temperature (middle) in the jet at set point sp03 shown in Table 1. The ETV source strength with CRAFT input is shown in the bottom.**

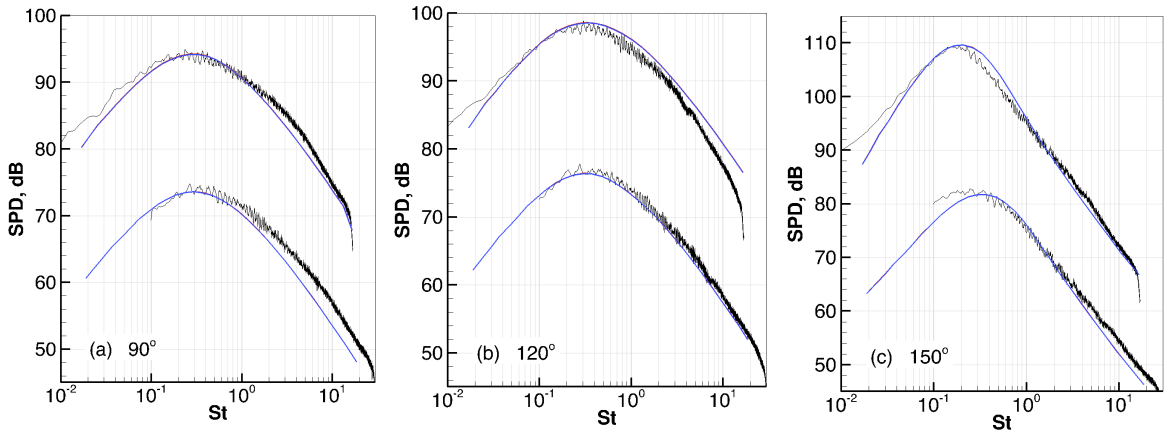


**Figure 16.** **Spectral predictions using CRAFT RANS input and empirical temperature variance (ETV) source model (blue); enthalpy variance source model (red); and measurements (dark) – Table 1, set points sp03 (bottom curves), sp07 (top curves) at inlet angles of: (a) 90°; (b) 120°; (c) 150°.**

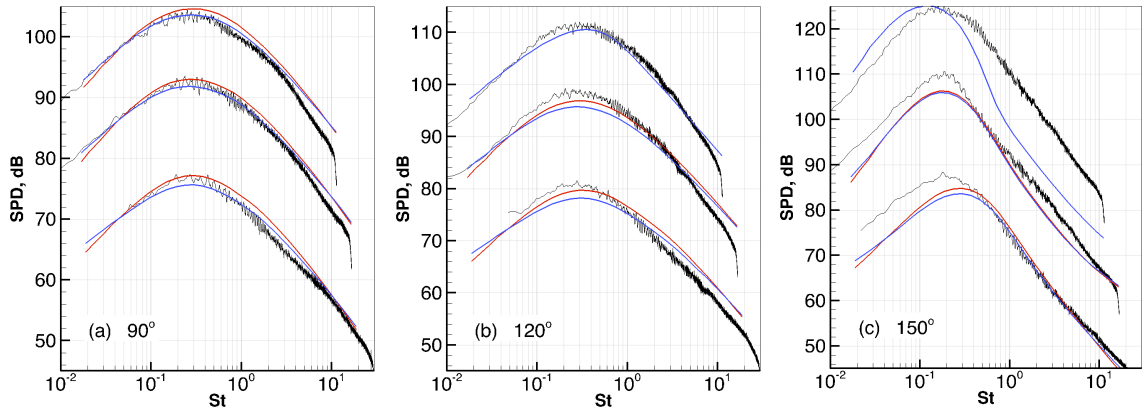


**Figure 17.** **Spectral predictions using CRAFT RANS input and empirical temperature variance (ETV) source model (blue); enthalpy variance source model (red); and measurements (dark) – Table 1, set points sp23 (bottom curves), sp27 (middle curves), sp29 (top curves) at inlet angles of: (a) 90°; (b) 120°; (c) 150°.**

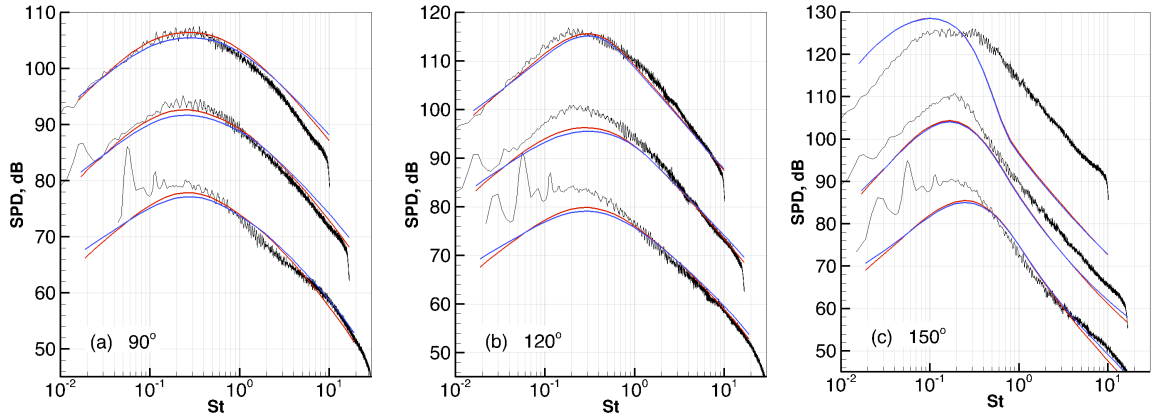


**Figure 18.** **Spectral predictions using CRAFT RANS input and empirical temperature variance (ETV) source model (blue); enthalpy variance source model (red); and measurements (dark) – Table 1, set points sp42 (bottom curves), sp46 (middle curves), sp49 (top curves) at inlet angles of: (a) 90°; (b) 120°; (c) 150°.**

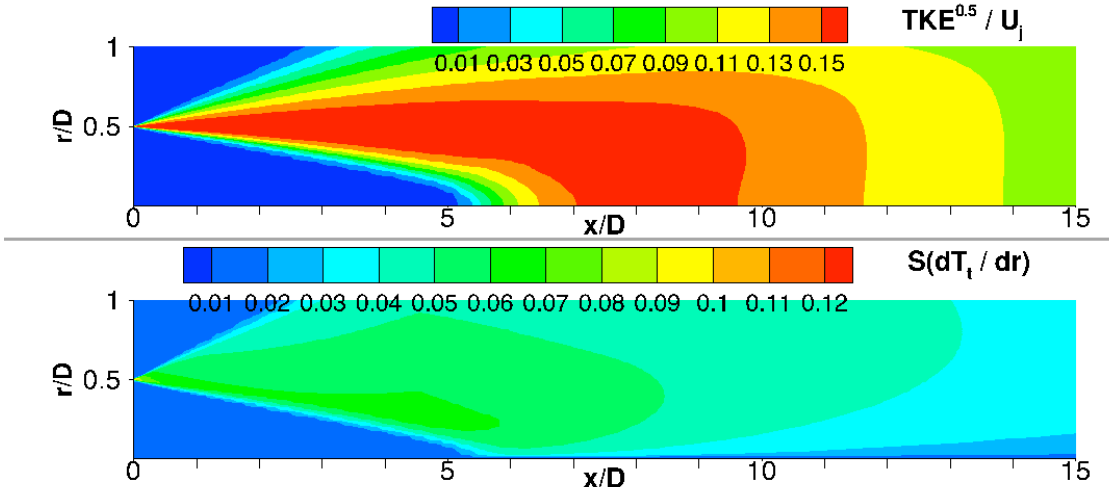


**Figure 19.** **Wind-US predictions for turbulent kinetic energy (top) and the ETV source strength (bottom) at set point sp23.**

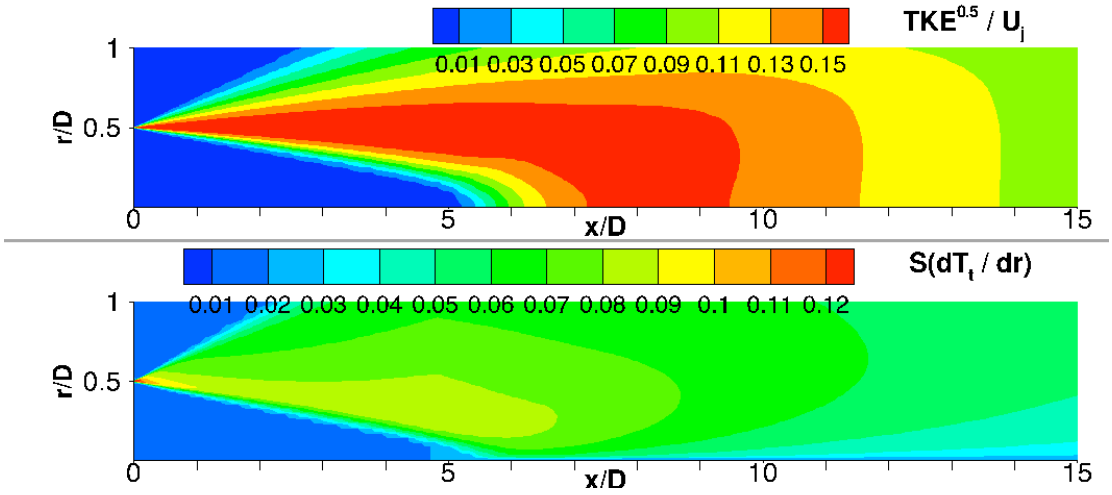


**Figure 20.** **Wind-US predictions for turbulent kinetic energy (top) and the ETV source strength (bottom) at set point sp237**

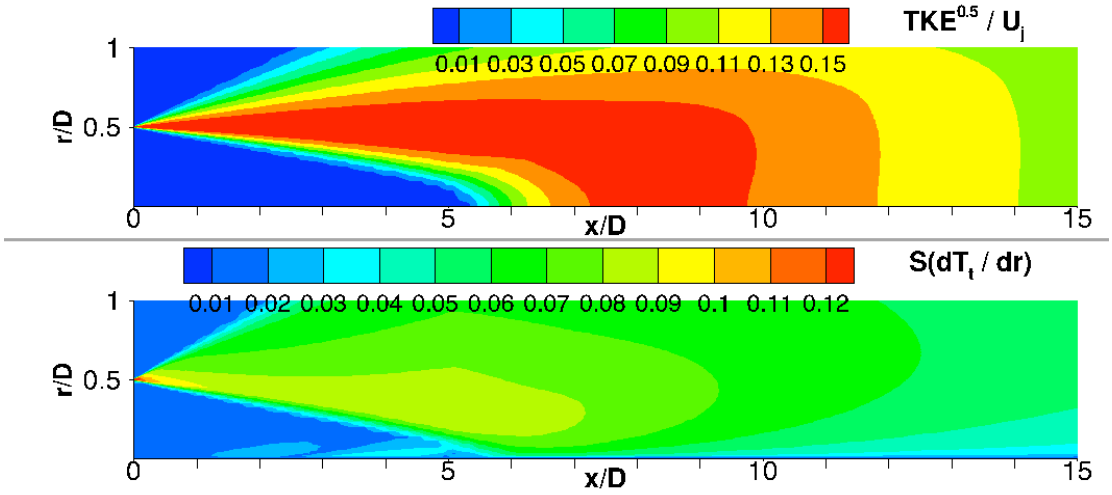


**Figure 21.** **Wind-US predictions for turbulent kinetic energy (top) and the ETV source strength (bottom) at set point sp29.**

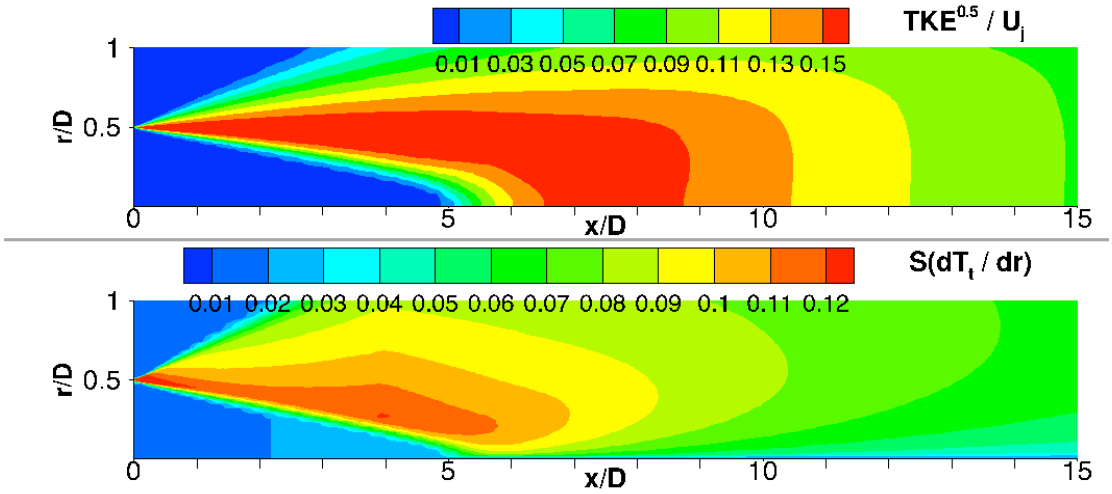


**Figure 22.** **Wind-US predictions for turbulent kinetic energy (top) and the ETV source strength (bottom) at set point sp42.**

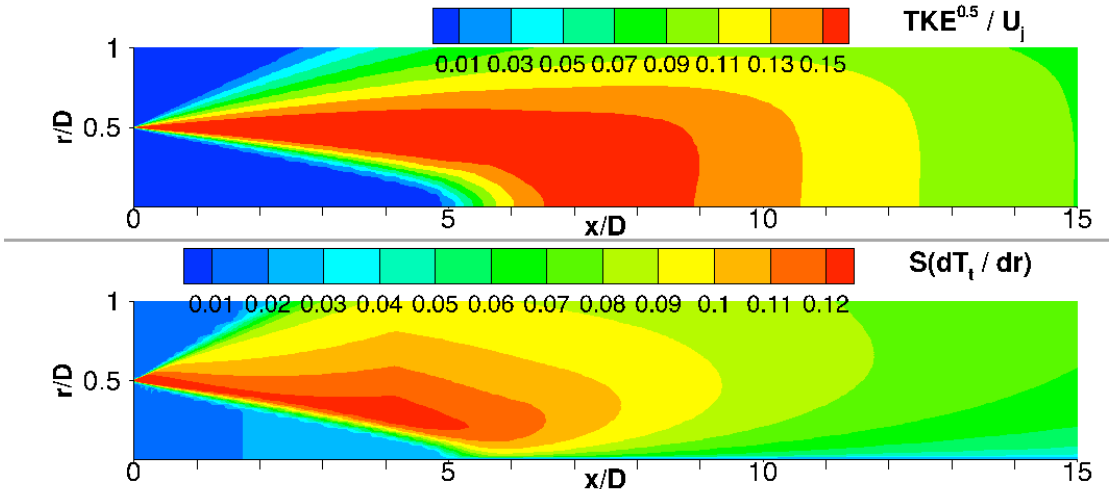


**Figure 23.** **Wind-US predictions for turbulent kinetic energy (top) and the ETV source strength (bottom) at set point sp23.**

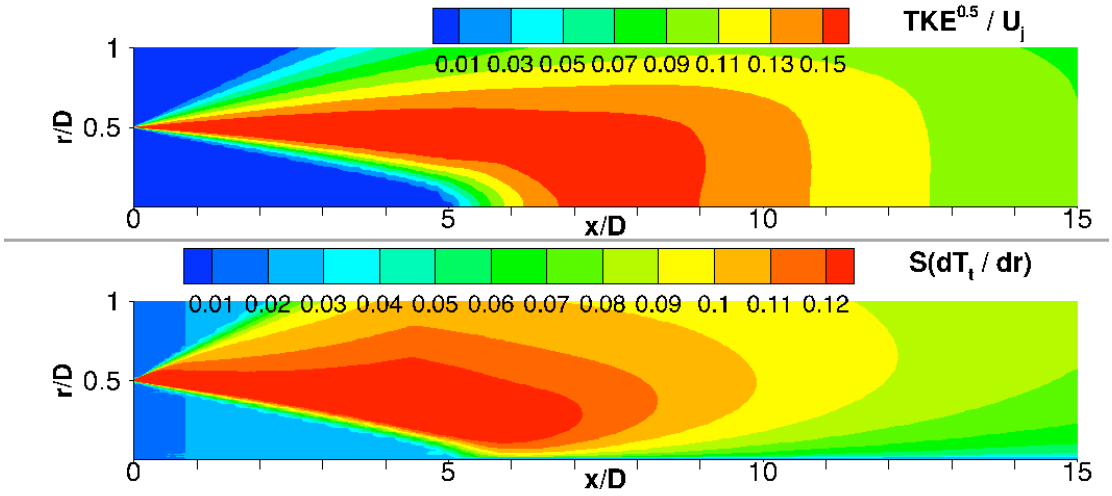


**Figure 24.** **Wind-US predictions for turbulent kinetic energy (top) and the ETV source strength (bottom) at set point sp49.**

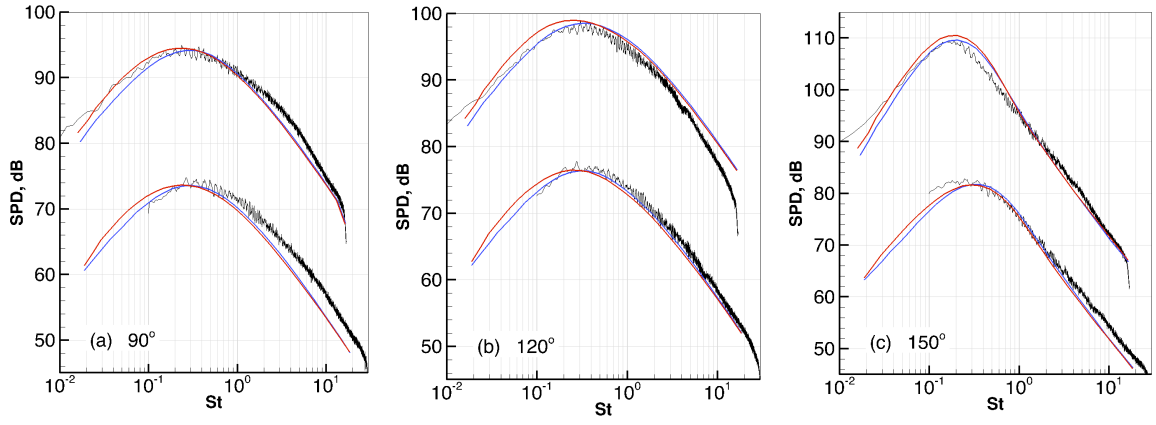


**Figure 25.** **Spectral predictions using Wind-US RANS input and ETV source model (red); CRAFT RANS input and ETV source model (blue); and measurements (dark) –Table 1, set points sp03 (bottom curves), sp07 (top curves) at inlet angles of: (a) 90°; (b) 120°; (c) 150°.**

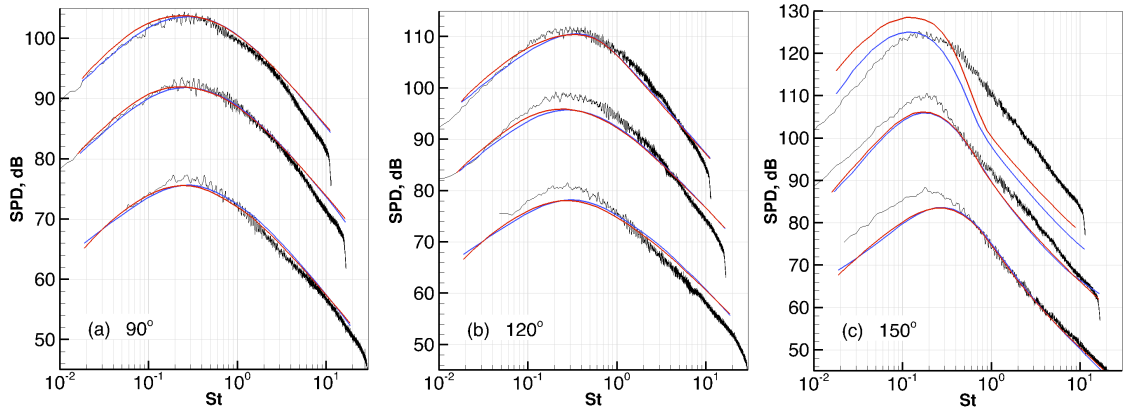


**Figure 26.** **Spectral predictions using Wind-US RANS input and ETV source model (red); CRAFT RANS input and ETV source model (blue); and measurements (dark) –Table 1, set points sp23 (bottom curves), sp27 (middle curves), sp29 (top curves) at inlet angles of: (a) 90°; (b) 120°; (c) 150°.**

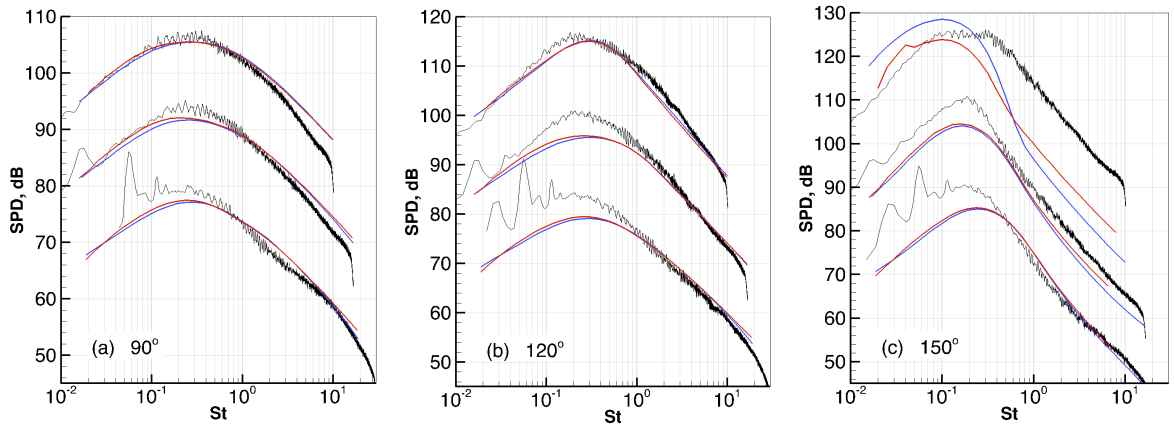


**Figure 27.** **Spectral predictions using Wind-US RANS input and ETV source model (red); CRAFT RANS input and ETV source model (blue); and measurements (dark) –Table 1, set points sp42 (bottom curves), sp46 (middle curves), sp49 (top curves) at inlet angles of: (a) 90°; (b) 120°; (c) 150°.**

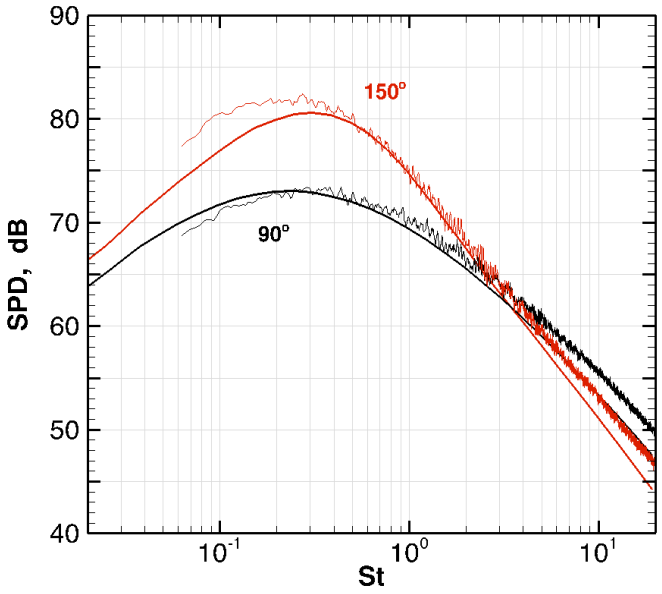


**Figure 28.** **Jet noise spectral predictions at inlet angles of 90° and 150° using Wind-US RANS input and ETV source model at Reading No. 1513, Table 2 (*NPR* =1.188, *NTR* = 1.04), (measurements are shown as jagged lines).**

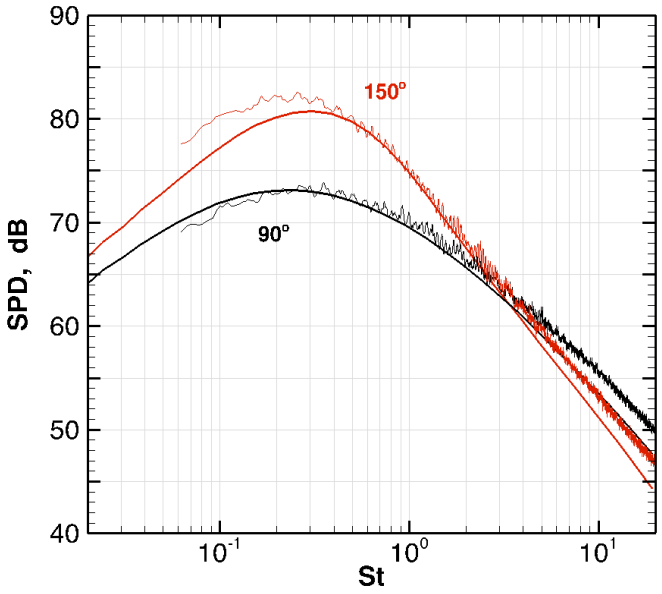


**Figure 29.** **Jet noise spectral predictions at inlet angles of 90° and 150° using Wind-US RANS input and ETV source model at Reading No. 1521 from Table 2 (*NPR* =1.188, *NTR* = 1.047).**

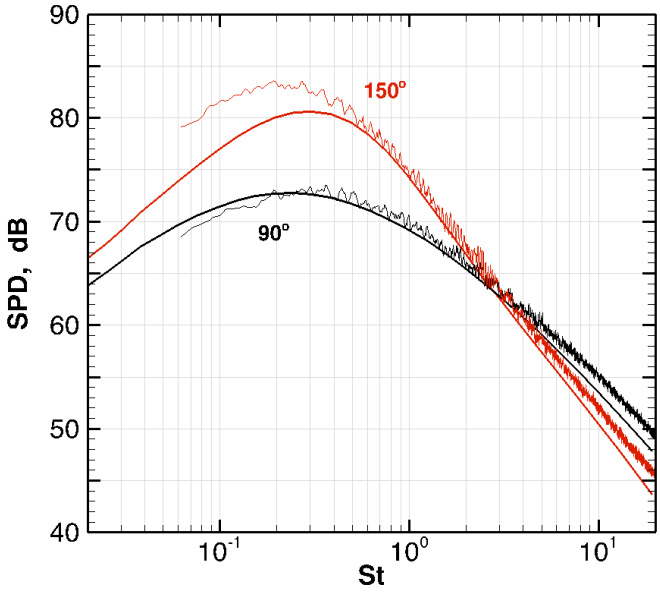


**Figure 30.** **Jet noise spectral predictions at inlet angles of 90° and 150° using Wind-US RANS input and ETV source model at Reading No. 1525 from Table 2 (*NPR* =1.168, *NTR* = 1.154).**

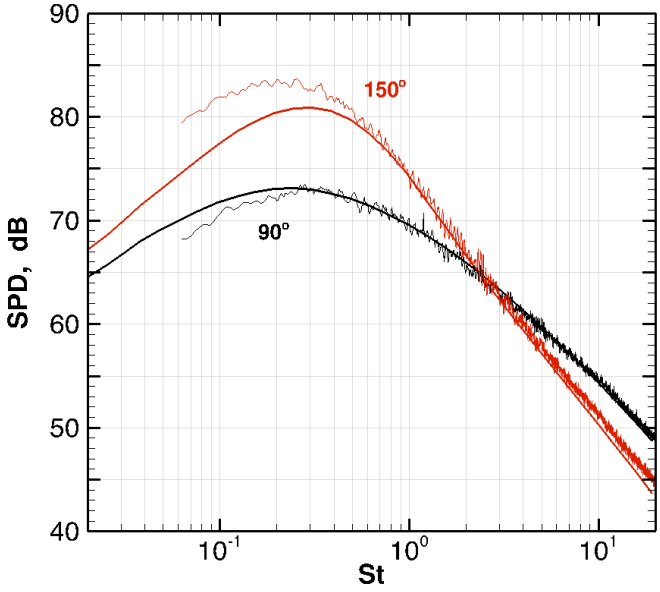


**Figure 31.** **Jet noise spectral predictions at inlet angles of 90° and 150° using Wind-US RANS input and ETV source model at Reading No. 1528 from Table 2 (*NPR* =1.153, *NTR* = 1.251).**

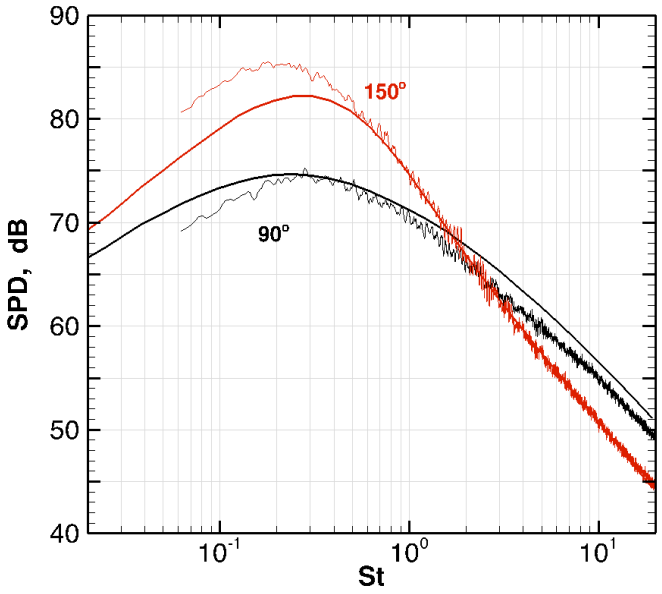


**Figure 32.** **Jet noise spectral predictions at inlet angles of 90° and 150° using Wind-US RANS input and ETV source model at Reading No. 1531 from Table 2 (*NPR* =1.128, *NTR* = 1.479).**

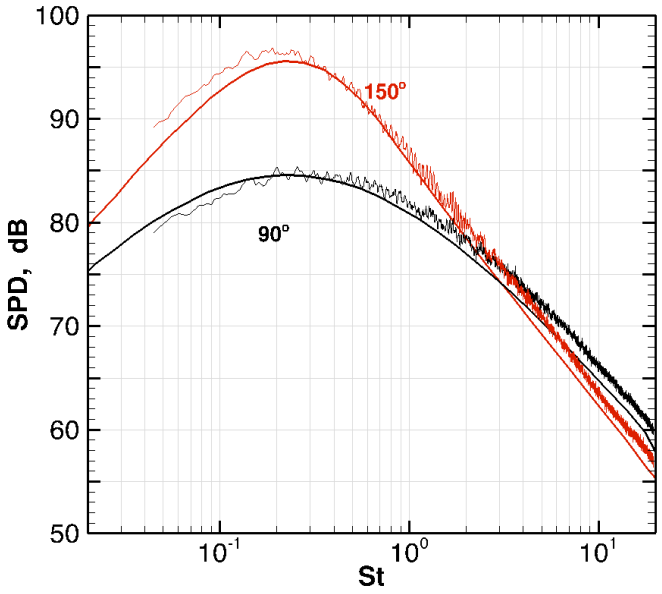


**Figure 33.** **Jet noise spectral predictions at inlet angles of 90° and 150° using Wind-US RANS input and ETV source model at Reading No. 1514 from Table 2 (*NPR* =1.418, *NTR* = 1.025).**

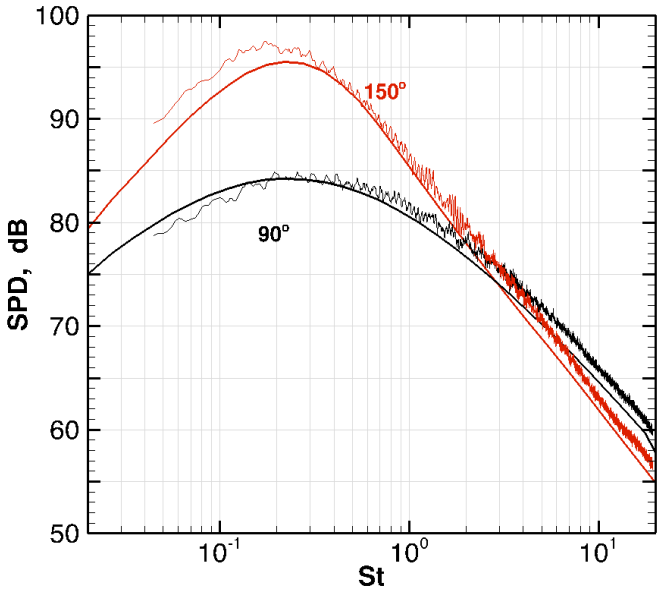


**Figure 34.** **Jet noise spectral predictions at inlet angles of 90° and 150° using Wind-US RANS input and ETV source model at Reading No. 1523 from Table 2 (*NPR* =1.389, *NTR* = 1.10).**

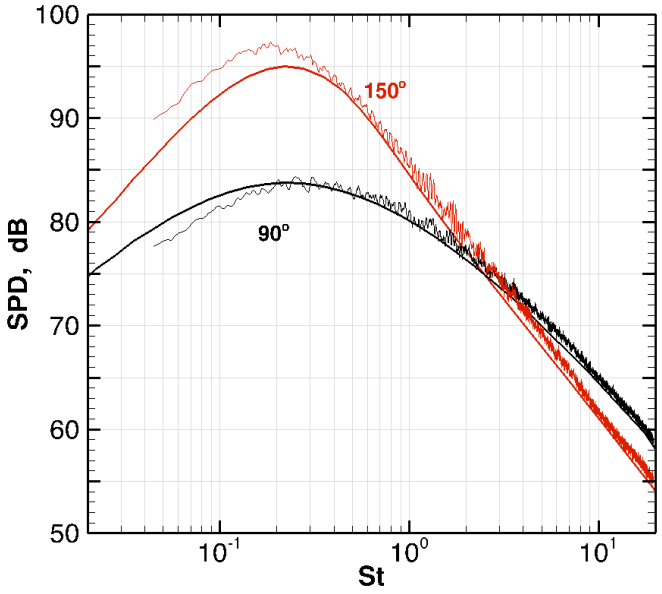


**Figure 35.** **Jet noise spectral predictions at inlet angles of 90° and 150° using Wind-US RANS input and ETV source model at Reading No. 1526 from Table 2 (*NPR* =1.345, *NTR* = 1.20).**

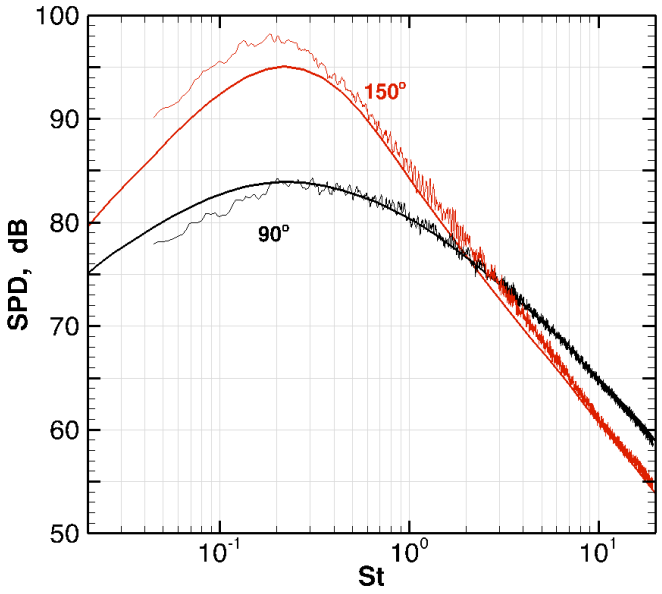


**Figure 36.** **Jet noise spectral predictions at inlet angles of 90° and 150° using Wind-US RANS input and ETV source model at Reading No. 1529 from Table 2 (*NPR* =1.318, *NTR* = 1.30).**

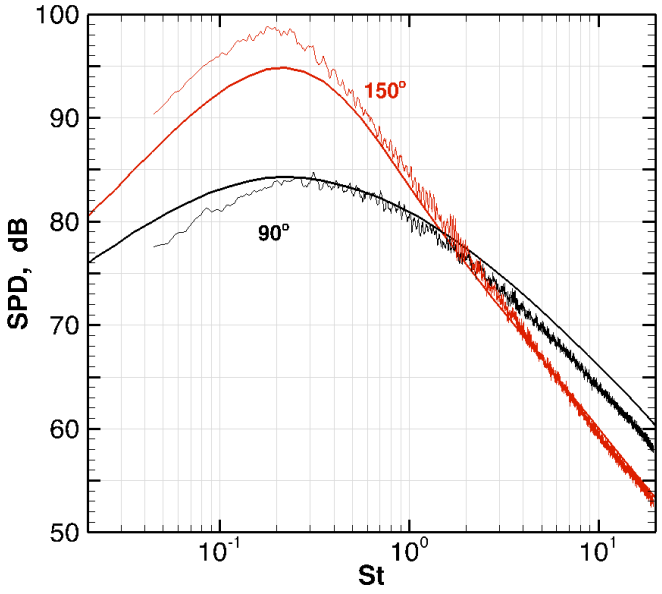


**Figure 37.** **Jet noise spectral predictions at inlet angles of 90° and 150° using Wind-US RANS input and ETV source model at Reading No. 1532 from Table 2 (*NPR* =1.26, *NTR* = 1.53).**

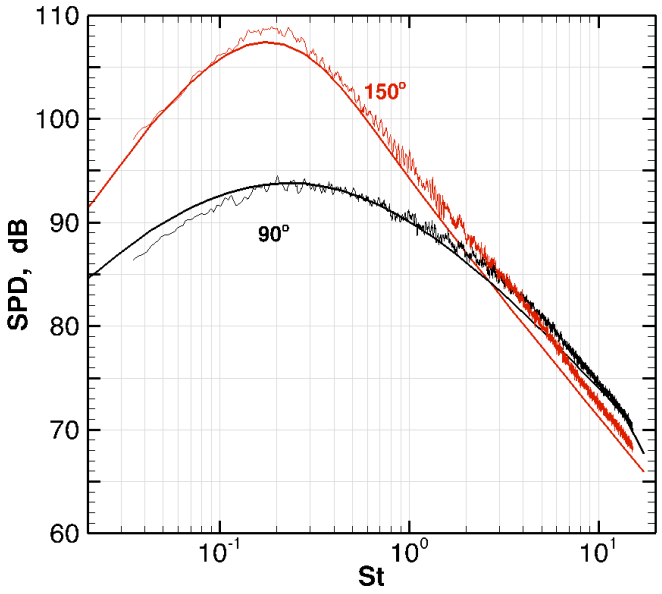


**Figure 38.** **Jet noise spectral predictions at inlet angles of 90° and 150° using Wind-US RANS input and ETV source model at Reading No. 1515 from Table 2 (*NPR* =1.834, *NTR* = 1.017).**

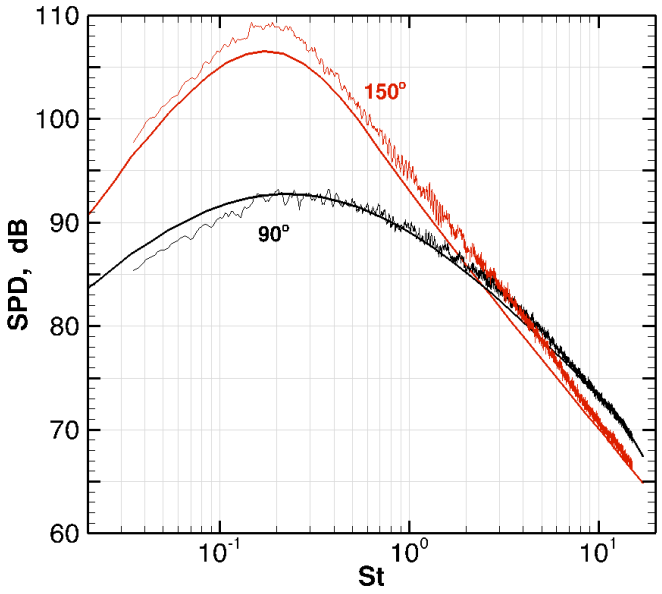


**Figure 39.** **Jet noise spectral predictions at inlet angles of 90° and 150° using Wind-US RANS input and ETV source model at Reading No. 1524 from Table 2 (*NPR* =1.694, *NTR* = 1.164).**

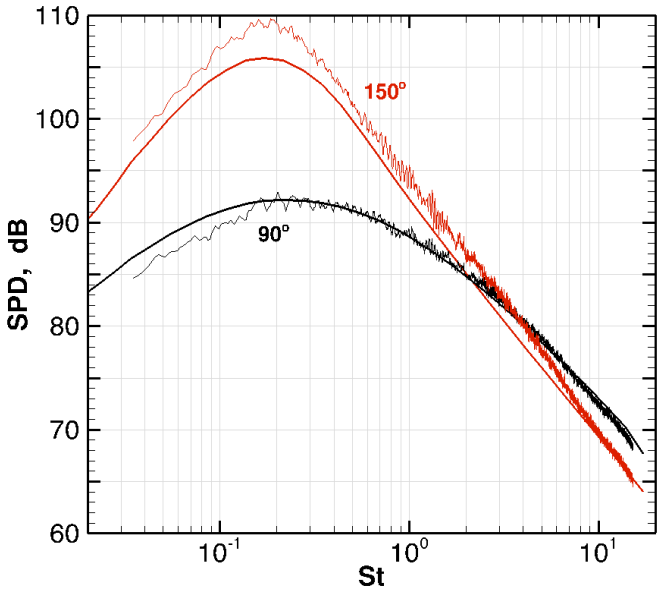


**Figure 40.** **Jet noise spectral predictions at inlet angles of 90° and 150° using Wind-US RANS input and ETV source model at Reading No. 1527 from Table 2 (*NPR* =1.616, *NTR* = 1.26).**

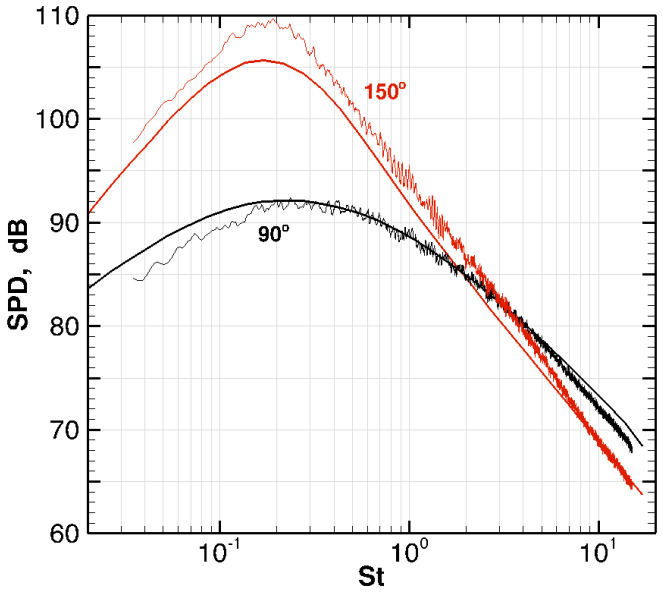


**Figure 41.** **Jet noise spectral predictions at inlet angles of 90° and 150° using Wind-US RANS input and ETV source model at Reading No. 1530 from Table 2 (*NPR* =1.563, *NTR* = 1.359).**

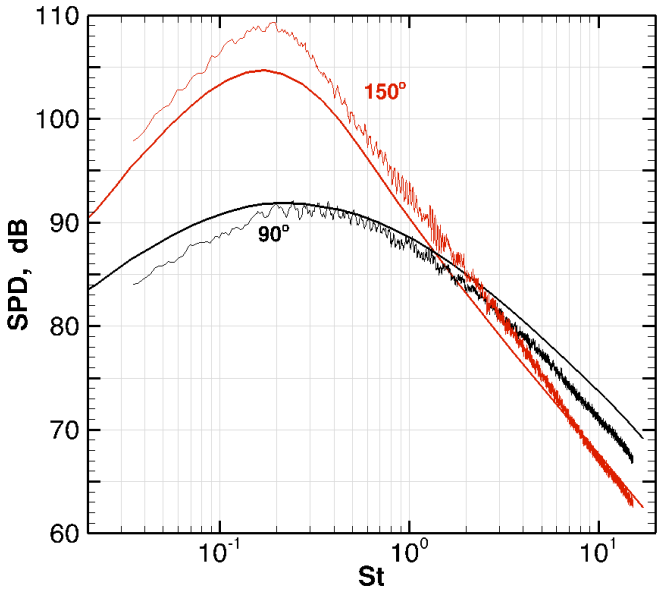


**Figure 42.** **Jet noise spectral predictions at inlet angles of 90° and 150° using Wind-US RANS input and ETV source model at Reading No. 1533 from Table 2 (*NPR* =1.452, *NTR* = 1.592).**

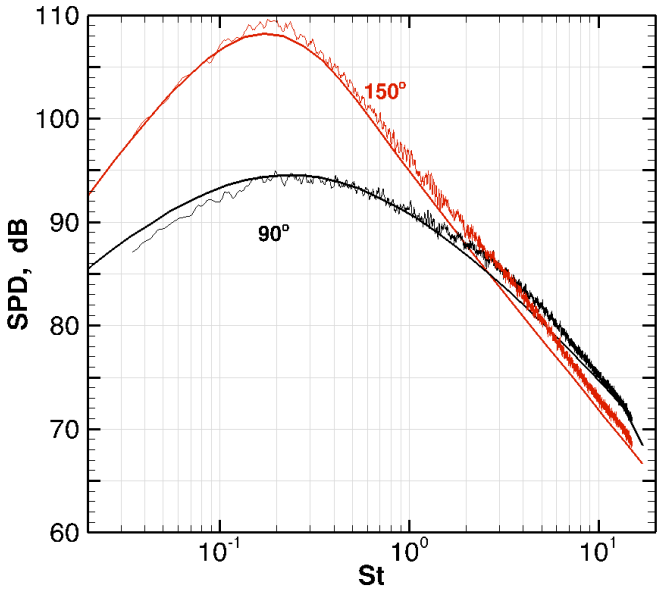


**Figure 43.** **Jet noise spectral predictions at inlet angles of 90° and 150° using Wind-US RANS input and ETV source model at Reading No. 1614 from Table 2 (*NPR* =1.893, *NTR* = 1.0).**

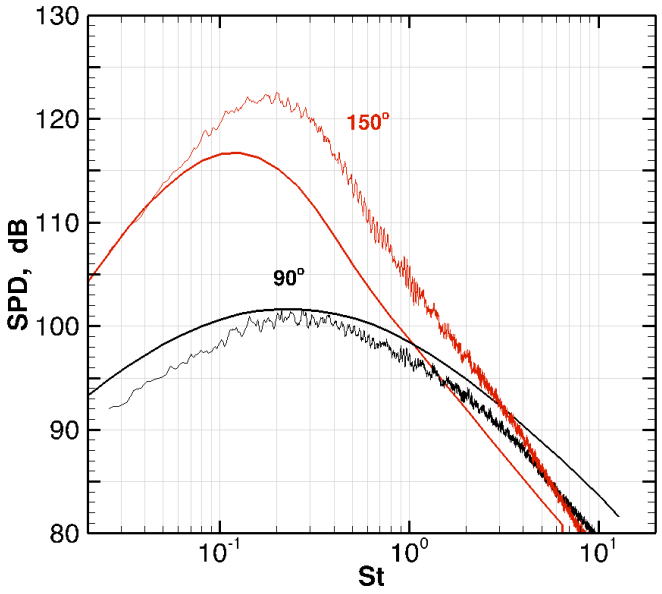


**Figure 44.** **Jet noise spectral predictions at inlet angles of 90° and 150° using Wind-US RANS input and ETV source model at Reading No. 1584 from Table 2 (*NPR* =1.893, *NTR* = 1.80).**

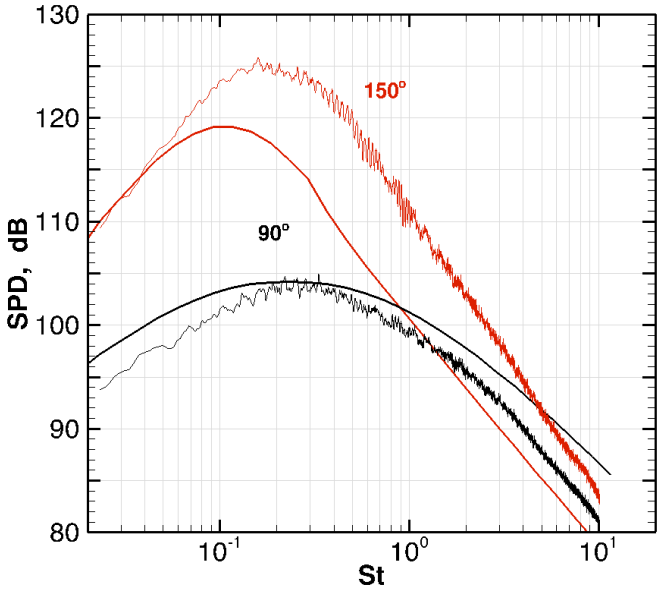


**Figure 45.** **Jet noise spectral predictions at inlet angles of 90° and 150° using Wind-US RANS input and ETV source model at Reading No. 1572 from Table 2 (*NPR* =1.893, *NTR* = 2.20).**

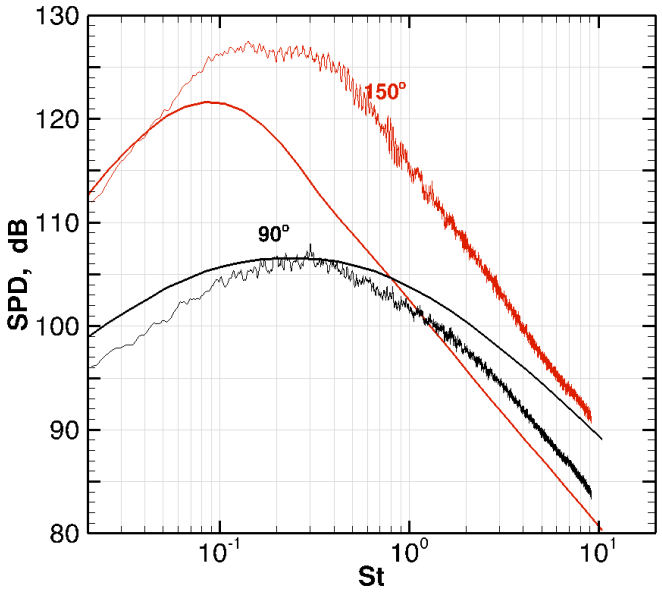


**Figure 46.** **Jet noise spectral predictions at inlet angles of 90° and 150° using Wind-US RANS input and ETV source model at Reading No. 1565 from Table 2 (*NPR* =1.893, *NTR* = 2.70).**

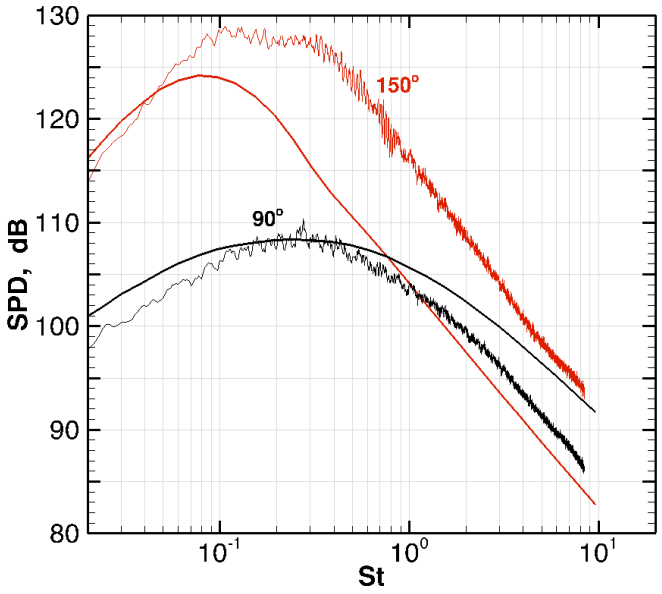


**Figure 47.** **Jet noise spectral predictions at inlet angles of 90° and 150° using Wind-US RANS input and ETV source model at Reading No. 1554 from Table 2 (*NPR* =1.893, *NTR* = 3.20).**

| REPORT DOCUMENTATION PAGE | Form Approved OMB No. 0704-0188 |
|---|---|



| 1. REPORT DATE *(DD-MM-YYYY)* | 2. REPORT TYPE | 3. DATES COVERED *(From - To)* |
|---|---|---|
| 01-10-2012 | Technical Memorandum | |

**4. TITLE AND SUBTITLE**
An Empirical Temperature Variance Source Model in Heated Jets

**5a. CONTRACT NUMBER**

**5b. GRANT NUMBER**

**5c. PROGRAM ELEMENT NUMBER**

**6. AUTHOR(S)**
Khavaran, Abbas; Bridges, James

**5d. PROJECT NUMBER**

**5e. TASK NUMBER**

**5f. WORK UNIT NUMBER**
WBS 561581.02.08.03.45.02.05

**7. PERFORMING ORGANIZATION NAME(S) AND ADDRESS(ES)**
National Aeronautics and Space Administration
John H. Glenn Research Center at Lewis Field
Cleveland, Ohio 44135-3191

**8. PERFORMING ORGANIZATION REPORT NUMBER**
E-18488

**9. SPONSORING/MONITORING AGENCY NAME(S) AND ADDRESS(ES)**
National Aeronautics and Space Administration
Washington, DC 20546-0001

**10. SPONSORING/MONITOR'S ACRONYM(S)**
NASA

**11. SPONSORING/MONITORING REPORT NUMBER**
NASA/TM-2012-217743

**12. DISTRIBUTION/AVAILABILITY STATEMENT**
Unclassified-Unlimited
Subject Category: 71
Available electronically at http://www.sti.nasa.gov
This publication is available from the NASA Center for AeroSpace Information, 443-757-5802

**13. SUPPLEMENTARY NOTES**

**14. ABSTRACT**
An acoustic analogy approach is implemented that models the sources of jet noise in heated jets. The equivalent sources of turbulent mixing noise are recognized as the differences between the fluctuating and Favre-averaged Reynolds stresses and enthalpy fluxes. While in a conventional acoustic analogy only Reynolds stress components are scrutinized for their noise generation properties, it is now accepted that a comprehensive source model should include the additional *entropy source* term. Following Goldstein's generalized acoustic analogy, the set of Euler equations are divided into two sets of equations that govern a non-radiating base flow plus its residual components. When the base flow is considered as a locally parallel mean flow, the residual equations may be rearranged to form an inhomogeneous third-order wave equation. A general solution is written subsequently using a Green's function method while all non-linear terms are treated as the equivalent sources of aerodynamic sound and are modeled accordingly. In a previous study, a specialized Reynolds-averaged Navier-Stokes (RANS) solver was implemented to compute the variance of thermal fluctuations that determine the enthalpy flux source strength. The main objective here is to present an empirical model capable of providing a reasonable estimate of the stagnation temperature variance in a jet. Such a model is parameterized as a function of the mean stagnation temperature gradient in the jet, and is evaluated using commonly available RANS solvers. The ensuing thermal source distribution is compared with measurements as well as computational result from a dedicated RANS solver that employs an enthalpy variance and dissipation rate model. Turbulent mixing noise predictions are presented for a wide range of jet temperature ratios from 1.0 to 3.20.

**15. SUBJECT TERMS**
Noise; Jet noise; Propulsion noise; Acoustics

| 16. SECURITY CLASSIFICATION OF: | | | 17. LIMITATION OF ABSTRACT | 18. NUMBER OF PAGES | 19a. NAME OF RESPONSIBLE PERSON |
|---|---|---|---|---|---|
| a. REPORT | b. ABSTRACT | c. THIS PAGE | | | STI Help Desk (email:help@sti.nasa.gov) |
| U | U | U | UU | 44 | 19b. TELEPHONE NUMBER *(include area code)* 443-757-5802 |